International Journal of Thermal Sciences 171 (2022) 107202

Contents lists available at ScienceDirect

International Journal of Thermal Sciences

journal homepage: www.elsevier.com/locate/ijts

A neural network model for free-falling condensation heat transfer in the presence of non-condensable gases

Eunho Cho [a,1], Haeun Lee [b,1], Minsoo Kang [b], Daewoong Jung [a], Geonhee Lee [b], Sael Lee [c], Chirag R. Kharangate [d], Huiun Ha [e], Sun Huh [e], Hyoungsoon Lee [a,b,*]

[a] School of Mechanical Engineering, Chung-Ang University, Seoul, 06974, Republic of Korea
[b] Department of Intelligent Energy and Industry, Chung-Ang University, Seoul, 06974, Republic of Korea
[c] Department of Software and Computer Engineering, Department of Artificial Intelligence, Ajou University, Suwon, 16499, Republic of Korea
[d] Mechanical and Aerospace Engineering Department, Case Western Reserve University, Cleveland, OH, 44106, USA
[e] Central Research Institute, Korea Hydro and Nuclear Power Co., Ltd., Daejeon, 34101, Republic of Korea

ARTICLE INFO

Keywords:
Condensation
Non-condensable gas
Free-falling
Artificial neural network
Multilayer perceptron
Passive containment cooling system

ABSTRACT

Condensation heat transfer has been widely studied for various applications such as power generation, water desalination, data centers, chemical and pharmaceutical syntheses, heating and air conditioning systems, and especially, the passive containment cooling system (PCCS) in nuclear power plants. The PCCS is designed to reduce the risk resulting from a loss of AC power or compounding human error. In a hypothetical accident situation, one of the main safety systems, the PCCS, condenses water vapor with gravity-driven force to remove the heat from the containment vessel. Although the condensation heat transfer in the presence of non-condensable gases for predicting the heat transfer performance of the PCCS has been successfully investigated, there is still no generalized model or correlation available. In this work, we focused on the development of universal models for predicting the heat transfer coefficients of free-fall condensation heat transfer on the external surfaces of vertical tubes in the presence of non-condensable gases. For this, we created a consolidated database covering a broad range of geometric values and operating conditions, including tube hydraulic diameter D_h = 10–41.2 mm, tube length L = 0.3–3.5 m, total pressure P_{tot} = 0.15–2.0 MPa, wall subcooling temperature ΔT_{sub} = 5–71 K, average condensation heat transfer coefficients of $90 \leq \overline{h} \leq 19{,}400$ W/m^{2}K, and Reynolds numbers of the film of $8 \leq Re_{film} \leq 7160$. We analyzed the influence of varying the geometric and operational parameter values by using this database. Conventional machine learning techniques such as nonlinear regression and multilayer perceptron (MLP) neural network methods were adopted to predict the condensation heat transfer rate based on the consolidated database. Moreover, the prediction accuracies of the condensation heat transfer rates of the proposed prediction models and 12 relevant correlations were compared by using the consolidated database. The proposed nonlinear regression model exhibited good prediction accuracy with a mean absolute error (MAE) of 12.7 % for average $\overline{h}$, which is much lower than those achieved by previously proposed relevant correlations. In addition, the MLP neural network model showed excellent prediction accuracy with an MAE of 4.2 % for the consolidated database.

1. Introduction

1.1. Passive cooling system for an innovative pressured water reactor

Since the Obninsk Nuclear Power Plant (Soviet Union), Calder Hall Reactor (England), and Shippingport Atomic Power Station (United States) were built in the 1950s, nuclear power plants have played a significant role in electricity generation. According to the World Energy Outlook (International Energy Agency, 2019) [1], nuclear energy supplies approximately 10 % of global electricity today; this supply level will be maintained for a while owing to the low level of carbon emissions and good cost–benefit tradeoff. However, the use of nuclear energy causes safety problems and has led to serious accidents. For example, the

* Corresponding author. School of Mechanical Engineering, Chung-Ang University, Seoul, 06974, Republic of Korea.
E-mail address: leeh@cau.ac.kr (H. Lee).
URL: http://atsla.cau.ac.kr (H. Lee).
[1] These authors contributed equally to this work.

https://doi.org/10.1016/j.ijthermalsci.2021.107202
Received 13 April 2021; Received in revised form 11 July 2021; Accepted 28 July 2021
Available online 13 August 2021

Nomenclature

ANN	artificial neural network
b	bias
C	coefficient
C_p	specific heat at constant pressure (J/kg·K)
D_{AB}	diffusion coefficient (cm^2/s)
D_h	hydraulic diameter (mm)
d	collision diameter (Å)
ΔT_{sub}	wall subcooling temperature (K)
Gr	Grashof number
g	gravitational acceleration (m/s^2)
h	heat transfer coefficient (W/m^2·K)
h_{fg}	latent heat (J/kg)
h*	dimensionless heat transfer coefficient
Ja	Jakob number
k	conductivity (W/m·K)
L	length (m)
M	molecular weight (g/mole)
MAE	mean absolute error
MLP	multilayer perceptron
N	number of data
OD	outer diameter (mm)
P	pressure (Pa)
PCCS	passive containment cooling system
R	Pearson correlation coefficient
$\mathrm{Re}_{\mathrm{film}}$	film Reynolds number
T_f	film temperature (K)
W	mass fraction
w	weight
X	mole fraction
Greek symbols	
β	expansion coefficient (K^{-1})
Γ	mass flow rate per unit film width (kg/m·s)
ε	potential well depth (eV)
θ	percentage of data with MAE within ±30 %
κ	Boltzmann constant (J/K)
μ	dynamic viscosity (kg/m·s)
ν	kinematic viscosity (m^2/s)
ξ	percentage of data with MAE within ±50 %
ρ	density (kg/m^3)
σ	surface tension (N/m)
Φ	Wilke viscosity weighing factor
ψ	node
Ω_D	collision integral
Superscripts	
–	average component
Subscripts	
c	critical
eff	effective
exp	experimental
f	liquid
g	vapor
i	interface
∞	ambient
nc	non-condensable gas
nu	Nusselt's theory
$plate$	flat plate
$pred$	predicted
r	reduced
sat	saturated
tot	total
$tube$	circular tube
v	water vapor
w	wall

Fukushima nuclear power plant accident was triggered by a magnitude 9.0 earthquake in 2011. The resulting meltdown caused many casualties and the long-term contamination of soil [2]. Therefore, radioactive contamination from unavoidable disasters should be mitigated to ensure the sustainable use of nuclear energy. In postulated accident situations, such as loss-of-coolant accidents (LOCAs), the failure of an active cooling system leads to an increasing amount of water vapor inside the containment. Simultaneously, water vapor condenses on the containment wall through the heat transfer to the outside. If the condensation heat transfer rate is less than the heat generation rate, the containment is pressurized; it may melt or explode, thereby leading to a catastrophic disaster in which the radioactive materials are directly discharged to the environment.

Innovative passive safety systems implemented in nuclear reactors can operate without any active interventions. Thus, the previously mentioned risks can be reduced in the event of a catastrophic system failure resulting from a loss of AC power or compounding human error. A passive containment cooling system (PCCS) is one of the featured passive safety designs for a pressurized water reactor; the PCCS uses gravitational force to supply coolants to ensure proper cooling and bring the reactor to a safe shutdown state during emergencies. Various PCCS designs have been proposed over the past few decades [3–8]. For instance, the AP600 [3] and AP1000 (Westinghouse Electric Company) [4] use a water tank that is installed higher than the containment system; the heat is removed from the external surface of the containment system. To minimize the conduction heat resistance during the heat transfer, the containment is made of steel with a high thermal conductivity. The Economic Simplified Boiling Water Reactor (ESBWR; GE Hitachi Nuclear Energy), Vodo–Vodyanoi Energetichesky Reactor-1200 (VVER-1200; Russia), Hualong Pressurized Reactor 1000 (HPR1000; China), and Innovative Power Reactor (iPOWER; Republic of Korea) adopted the alternative PCCS design with concrete, which is a low-conductivity material [5–8]. The PCCS in the ESBWR [5] consists of multiple tubes directly submerged in a large water pool; the heat is removed while the discharged steam with non-condensable gases condenses inside the tubes. The PCCSs of the VVER-1200 [6], HPR1000 [7], and iPOWER [8] use multiple tubes installed inside the containment; these tubes are coupled to a highly located water reservoir outside the containment system. In a postulated situation, the condensation occurs outside the tubes, while the water coolant inside the tubes is circulated by the gravity-driven buoyancy flow caused by the increasing temperature of the water. In this system, the cooling performance of the PCCS strongly depends on the condensation heat transfer rate on the external surface of the tubes and the relative location between the tubes and water reservoir [9].

1.2. Heat transfer across free-falling condensed liquid film

Condensed, free-falling films are characterized by laminar, wavy–laminar, and turbulent flow regimes with different heat transfer characteristics according to the film Reynolds number [10] (see Fig. 1). In 1916, Nusselt [11] proposed a theoretical prediction model for laminar film condensation, which considers the thermo-physical properties of the working fluid and condensation length:

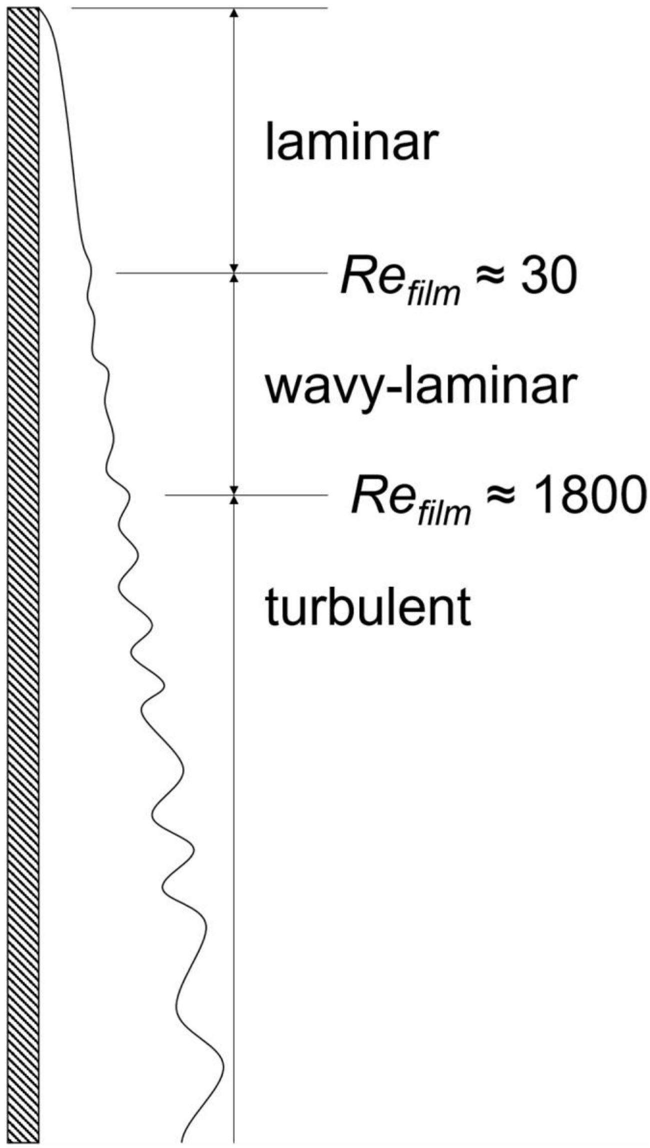

Fig. 1. The free-falling condensed liquid film flow regime.

$$\overline{h} = 0.943\left[\frac{g\rho_f(\rho_f-\rho_g)k_f^3h'_{fg}}{\mu_f L\Delta T_{sub}}\right]^{1/4} \tag{1}$$

where h'_{fg} is the modified latent heat given by $h'_{fg} = h_{fg} + 0.68C_{p,f}\,\Delta T_{sub}$ for a nonlinear temperature profile [12]. For $\rho_f \gg \rho_g$, Eq. (1) can be written in the following form:

$$h^* = \frac{\overline{h}}{k_f}\left(\frac{\nu_f^2}{g}\right)^{1/3} = 1.47Re_{film}^{-1/3} \tag{2}$$

where h^* is the dimensionless average heat transfer coefficient, and Re_{film} is the film Reynolds number:

$$Re_{film} \equiv \frac{4\Gamma}{\mu_f} = \frac{4}{\mu_f}\frac{\overline{h}L\Delta T_{sub}}{h'_{fg}} \tag{3}$$

Although the Nusselt model is well known for accurately predicting the condensation heat transfer coefficient in the laminar regime, it tends to underpredict the heat transfer coefficient in the wavy–laminar regime by not accounting for the interfacial wave effect [13]. Many researchers have suggested modified models applicable to wavy–laminar or turbulent flow regimes by considering the effects of waves or turbulence with an empirical correction factor based on experimental data [14–20].

In a PCCS for the safety of nuclear power plants, the condensation heat transfer does not occur around the pure working fluid; it occurs around the non-condensable gas mixed with the fluid. In the containment of a PCCS, the air is generally mixed with water vapor at high concentrations, thereby resulting in a relatively low condensation heat transfer rate [21]. Unlike for a condensation system in pure water vapor, diffusion is a dominant factor for the condensation heat transfer in the presence of non-condensable gas. Because water vapor partially condenses on the wall in a large vessel, the concentration difference of the water vapor is developed by the condensation mass transfer rate. Thus, the water vapor concentration gradient induces the diffusion of water vapor through the space between non-condensable gas molecules. Dehbi [22] investigated the effects of the air fraction on the water vapor condensation with a copper tube in an insulated vessel. The condensation heat transfer coefficients were measured for an air mass fraction range of $W_{nc} = 0.25$–0.9 with a copper tube with 38 mm-OD and 3.5 m length. Liu *et al.* [23] conducted a water vapor condensation heat transfer experiment for air mass fractions of $W_{nc} = 0.21$–0.75 with an OD of 40 mm and 2 m long copper tube. Ahn [24] and Kim *et al.* [25] experimentally investigated the effects of pressure on the condensation heat transfer in the presence of nitrogen. An autoclave chamber with an OD of 40 mm and 0.6 m long copper tube located at its center was used for pressurizing up to 2.0 MPa with nitrogen. The researchers reported that the condensation heat transfer coefficients decreased with increasing nitrogen mass fraction. Moreover, Kawakubo *et al.* [26] used an OD of 12 mm and 1 m long SS304 tube. The heat transfer coefficients were determined for an air mass fraction range of 0.08–0.62 and total pressure range of 0.2–0.4 MPa. Su *et al.* [27,28] used an equivalent experimental setup with an air and water vapor mixture and an OD of 38 mm and 2 m long tube; the condensation heat transfer was studied for a wall subcooling temperature range of 13–70 K. Tong *et al.* [29] measured the condensation heat transfer coefficients in the presence of air with an OD of 38 mm and 2 m long smooth stainless steel tube and finned tube. They reported that the condensation heat transfer coefficients on the smooth tube were higher than those of the finned tube when the air mass fraction was less than 0.4. Furthermore, both Lee *et al.* [30] and Jang *et al.* [31] used 1 m long SS304 tube with OD of 40 mm and 10 mm and determined the condensation heat transfer coefficients for an air mass fraction of $W_{nc} = 0.1$–0.81 at a total pressure of $P_{tot} =$ 0.2–0.5 MPa. Fan *et al.* [32,33] compared the condensation heat transfer coefficients of a smooth and corrugated tube (an OD of 32.1 mm and 2 m length) with and without air.

1.3. Machine leaning for investigating heat transfer

Machine learning approaches such as Decision Tree, Artificial Neural Networks, Deep Learning, and Genetic Programming have been spotlighted in the fields of predicting or decision-making for complicated systems since the early 1980s [34–38]. In particular, the ANN, which was proposed by McCulloch and Pitts [39], was inspired by the human brain system and, in combination with the backpropagation algorithm [40,41], has regained popularity. In addition, ANNs have received considerable attention in the field of heat transfer owing to their superior prediction accuracy and easy assessment compared to those of conventional empirical and semi-empirical correlations or computational fluid dynamics (CFD). The conventional regression method based on experimental analyses is the most accurate for the specific geometrical and operating conditions under which experiments are conducted; however, its prediction accuracy is usually drastically reduced under different geometrical or operating conditions. The CFD method is often adopted to predict accurately complex geometries; however, it cannot accurately predict condensation heat transfer and causes extremely high computational costs [42]. By contrast, ANNs accurately predict the system performance at much lower computational costs owing to their ability to learn the interrelationships between

Table 1
Details of consolidated database with data from water vapor free-falling condensation with non-condensable gases.

Author(s)	Non-condensable gas	L [m]	D_h [mm]	P_{tot} [MPa]	ΔT_{sub} [K]	W_{nc}	Re_{film}	Data points (pure water vapor)	Uncertainty of $\overline{h}$ [%]
Dehbi (1991) [22]	Air	1.16–3.5	38	0.15–0.46	9–47	0.25–0.9	8–1230	216	14.3
Liu *et al.* (2000) [23]	Air	2	40	0.25–0.46	7–33	0.21–0.75	40–840	26	18
Ahn (2007) [24]	Nitrogen	0.6	38	0.4–1.2	53–61	0.09–0.69	130–1330	9	–
Kim *et al.* (2009) [25]	Nitrogen	0.65	41.2	0.4–2.0	55–60	0.01–0.72	60–3410	72	25
Kawakubo *et al.* (2009) [26]	Air	0.33–1	12	0.2–0.4	5–52	0.08–0.62	30–800	45	26
Su *et al.* (2013) [27]	Air	2	38	0.2–0.6	27–69	0.23–0.6	240–1610	119	15
Su *et al.* (2014) [28]	Air	2	38	0.4–0.6	13–26	0.07–0.74	130–1700	31	19.6
Tong *et al.* (2015) [29]	Air	2	38	0.2–0.6	5–55	0–0.78	70–6570	50 (16)	14.6
Lee *et al.* (2017) [30]	Air	1	40	0.2–0.5	19–69	0.1–0.81	20–580	43	13.6
Jang *et al.* (2018) [31]	Air	1	10	0.2–0.5	30–47	0.1–0.75	70–990	18	21.4
Fan *et al.* (2018a,b) [32, 33]	Air	2	32	0.2–0.5	12–71	0–0.79	70–7160	227 (14)	11.8 for 2018a

variables. However, their principal deficiency is that the decision-making process cannot be explained by the underlying heat transfer physics.

Despite not being able to comprehend the decision process, some researchers have achieved successful and meaningful progress by studying the single-phase heat transfer with ANNs [43–48]. For instance, Jambunathan *et al.* [43] used commercial ANN software to predict the transient convective heat transfer coefficients of the interior of a duct. Pacheco-Vega *et al.* [44] correlated the heat transfer rates of air and R22 of a fin-and-tube heat exchanger with an ANN and a cross-validation method [49], which is suitable for a limited amount of experimental data. Furthermore, Islamoglu and Kurt [45] used an ANN to correlate the coefficients of forced convection heat transfer in a corrugated channel. Ghahdarijani *et al.* [46] predicted the heat transfer and pressure drop of nanofluids in a double-walled reactor. Naphon *et al.* [47] investigated the influences of jet impingement on the heat transfer and pressure drop of a nanofluid in a microchannel with ANN and CFD approaches. Lee *et al.* [48] developed an ANN model for predicting the thermal performance efficiently by predicting the frictional pressure drop in the micro-pin fin heat sink. More recently, ANNs were adopted to evaluate the two-phase heat transfer in various applications; the methods exhibited superior prediction accuracies compared to those of conventional regression models [50–56]. For instance, Balcilar *et al.* [50] analyzed the condensation heat transfer coefficients and pressure decreases of R134a in a mini vertical tube with an ANN. Azizi and Ahmadloo [51] developed an ANN to study the condensation heat transfer coefficients in an inclined tube with 440 experimentally determined data points; the mean absolute error (MAE) was below 2 %. Khosravi *et al.* [52] used an ANN to correlate the evaporation pressure decrease of R407C in two mini tubes of different diameters. The mass flux, tube diameter, saturation pressure, and vapor quality were used as input parameters; the approach led to well-fitted results. Parrales *et al.* [53] proposed two ANN models for predicting the heat transfer coefficient values of a vertical helical evaporator; they analyzed the sensitivity levels of the input variables and showed good predictions of the experimental data. Qiu *et al.* [54] predicted the flow boiling heat transfer coefficients of mini/micro channels with an ANN. The researchers optimized the ANN architecture with 16,953 data points by considering the influence of the input parameter sets on the predictability; the MAE was 14.3 % with a dimensionless parameter group as input parameter set, which is considerably better than the results of conventional correlations. Recently, Zhou *et al.* [55] developed ANN, Random Forest, Adaptive Boosting, and Extreme Gradient Boosting models to predict the condensation heat transfer coefficients in mini/-micro channels with 4882 data points. The researchers reported that ANN model showed the best prediction with the MAE of 6.8 %. Zhu *et al.* [56] investigated flow boiling and condensation heat transfer in mini channels; they correlated the heat transfer coefficient values of R134a in channels with serrated fins and obtained good predictions for boiling and condensation with mean absolute relative deviations of 11.4 % and 6.1 %, respectively.

1.4. Objectives of study

The condensation heat transfer characteristics in the presence of non-condensable gases have been successfully investigated over the last three decades. However, there remains a lack of a generalized model or correlation for predicting the condensation heat transfer coefficients with non-condensable gas since most previous studies have been conducted under very narrow geometrical and operational variations. The present study focuses on the development of universal models for predicting the heat transfer coefficients of free-fall condensation heat transfer on the external surfaces of vertical tubes in the presence of non-condensable gases covering broad ranges of geometrical and operating conditions. For this, we created a consolidated database of 856 data points of the condensation heat transfer on vertical tubes in the presence of non-condensable gases or pure water vapor only was prepared, and the influences of geometrical and operational variations were investigated. In addition, new predictive tools using the conventional nonlinear regression and ANN approaches for the accurate prediction of condensation heat transfer coefficients in the presence of non-condensable gases are proposed. The prediction accuracies of the two proposed models were compared with those of previous relevant correlations based on the consolidated database.

2. Methods

2.1. Database constructed from experimental study of film condensation

A consolidated database was prepared by using 856 experimental data points of free-falling film condensation measurements on the external surfaces of circular tubes originating from 12 research sources published over the past three decades [22–33]. The geometrical and operational parameters such as the tube length, hydraulic diameter, non-condensable gas mass fraction, total pressure, and wall subcooling temperature were directly extracted. Subsequently, the thermo-physical properties and film Reynolds number were determined based on the saturation temperature of the vapor and film temperature of the liquid. Table 1 lists the detailed geometries and operating conditions presented in the databases in chronological order.

The consolidated database covers broad ranges of geometrical and operating conditions: $D_h = 10$–41.2 mm, $L = 0.3$–3.5 m, $P_{tot} = 0.15$–2.0 MPa, $\Delta T_{sub} = 5$–71 K, $90 \leq \overline{h} \leq 19{,}400$ W/m^2·K, and $8 \leq Re_{film} \leq 7160$. In addition, the database only included data for the external surfaces of vertical circular tubes, and data for plates and internal and horizontal flow were excluded. In total, 856 data points, including 30 data points for pure water vapor and 826 data points for water vapor with non-condensable gases with mass fractions of $W_{nc} = 0$–0.9 were included.

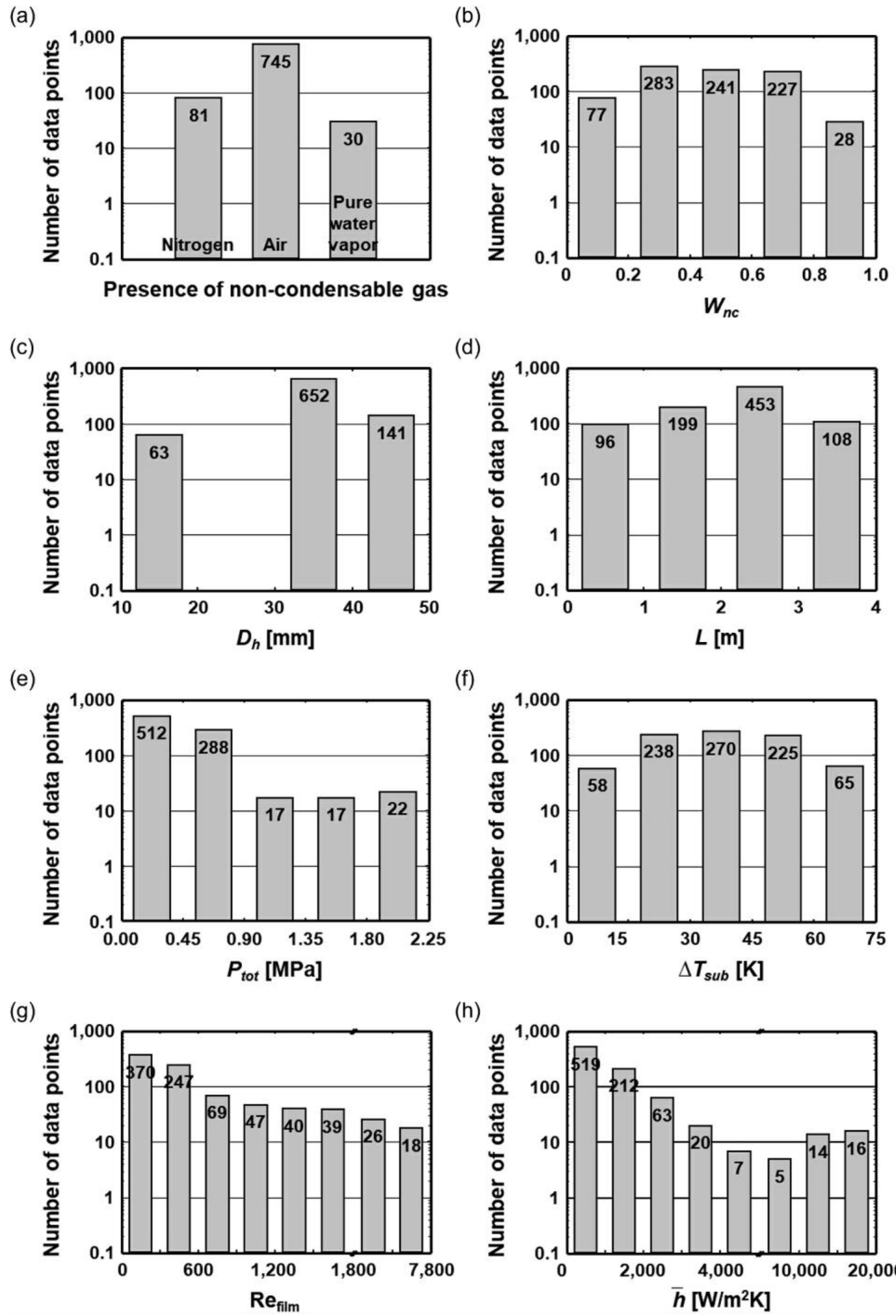

Fig. 2. Distribution of the number of data points relative to (a) the presence of non-condensable gas, (b) the mass fraction of non-condensable gas (W_{nc}), (c) the hydraulic diameter of the tube (D_h), (d) the tube length (L), (e) the total pressure (P_{tot}), (f) the wall subcooling temperature (ΔT_{sub}), (g) the film Reynolds number (Re_{film}), and (h) the average heat transfer coefficient ($\bar{h}$).

$$\frac{W_{nc}}{1-W_{nc}} = \frac{W_{nc}}{W_v} = \frac{M_{nc}P_{nc}}{M_v P_v} = \frac{M_{nc}}{M_v}\left(\frac{P_{tot}-P_v}{P_v}\right) \tag{4}$$

where W is the mass fraction, and M is the molecular weight; the subscripts nc and v represent the non-condensable gas and water vapor, respectively.

Fig. 2 shows the distributions of the data points according to the (a,b) non-condensable gas, (c,d) geometrical conditions, and (e–h) operating conditions. Data from two different non-condensable gases were included in the database: 81 nitrogen data points from Ahn [24] and Kim *et al.* [25] and 745 data points for air from Dehbi [22], Liu *et al.* [23], Kawakubo *et al.* [26], Su *et al.* [27,28], Tong *et al.* [29], Lee *et al.* [30], Jang *et al.* [31], and Fan *et al.* [33]. In addition, 30 data points for pure water vapor from Tong *et al.* [29] and Fan *et al.* [32] were included to increase the prediction accuracy for low non-condensable gas mass fractions during training. In the consolidated database, 92.6 % of the data points originate from tubes with $30 \leq D_h < 50$ mm while only 7 % originate from tubes with $D_h < 20$ mm. Most data points (93.5 %) in the database correspond to a relatively low P_{tot} of $<$0.9 Mpa, with 56 of them falling into $P_{tot} \geq 1.2$ MPa. Most of the 856 data points correspond to $30 \leq Re_{film} < 1{,}800$, which are in the wavy–laminar flow regime, while 20 and 44 data points correspond to the laminar ($Re_{film} < 30$) and turbulent ($Re_{film} > 1800$) flow regimes, respectively. Owing to the presence of non-condensable gases, most $\bar{h}$ values are concentrated (< 2000

Table 2
Thermo-physical and operating ranges of data in consolidated database.

T_{sat} [°C]	ρ_f [kg/m^3]	ρ_g [kg/m^3]	$\mu_f \times 10^4$ [kg/m·s]	$\mu_g \times 10^4$ [kg/m·s]	k_f [W/m·K]	k_g [W/m·K]	$C_{p,f}$ [J/kg·K]	$C_{p,g}$ [J/kg·K]	h_{fg} [kJ/kg]	σ [N/m]	Re_{film}
62–210	887–988	0.15–9.6	1.5–5.5	0.11–0.16	0.64–0.68	0.022–0.042	4182–4405	1969–3153	1899–2352	0.036–0.065	8–7160

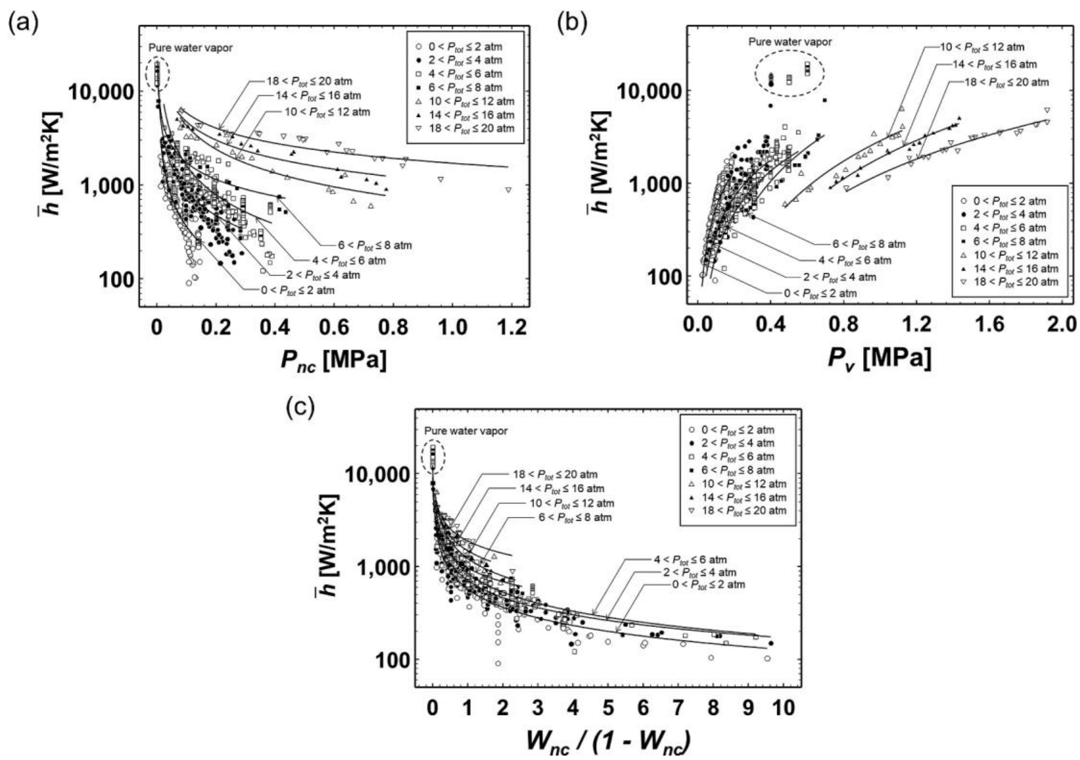

Fig. 3. Variations in average heat transfer coefficient ($\bar{h}$) from the consolidated database with respect to (a) partial pressure of non-condensable gas (P_{nc}), (b) partial pressure of water vapor (P_v), and (c) the ratio of non-condensable gas to water vapor mass fractions (W_{nc}/(1-W_{nc}).

W/m^2·K).

Table 2 provides details about the ranges of the experimental data. The parameters extracted from the databases are as follows:

- Types of non-condensable gases: air and nitrogen;
- Mass fraction of non-condensable gas: $W_{nc} = 0$–0.9;
- Hydraulic diameter of tube $D_h = 10$–41.2 mm;
- Tube length $L = 0.3$–3.5 m;
- Total pressure $P_{tot} = 0.15$–2.0 MPa;
- Wall subcooling temperature $\Delta T_{sub} = 5$–71 K;
- Film Reynolds number $Re_{film} = 8$–7160
- Average convective heat transfer coefficient $\bar{h} = 90$–$19{,}400$ W/m^2·K.

2.2. Thermal modeling of condensation heat transfer

Two different approaches were used to predict the coefficients of the condensation heat transfer on the external surface of a vertical tube in the presence of non-condensable gases. First, an empirical correlation was established with the conventional nonlinear regression method. Second, the multilayer perceptron (MLP) neural network was adopted to obtain better predictions [34].

2.2.1. New correlation based on nonlinear regression model

Fig. 3 shows the variations in the average heat transfer coefficients of the consolidated database with respect to the (a) partial pressure of the non-condensable gas (P_{nc}), (b) partial pressure of the water vapor (P_v), and (c) ratio of non-condensable gas to water vapor mass fractions (W_{nc}/(1-W_{nc})). The solid curves in Fig. 3 represent the regression curves of the heat transfer coefficients over different P_{tot} ranges of the consolidated database. They were plotted to investigate the effect of P_{tot} on the condensation heat transfer without considering the pure-water vapor data. As shown in Fig. 3, the heat transfer coefficients decrease with increasing P_{nc} and increase with increasing P_v. In addition, the heat transfer coefficients decrease with increasing W_{nc}/(1-W_{nc}), which corresponds to the observations reported in Refs. [57–59]. These trends are mainly due to the effects of (i) the partial pressure of the water vapor, (ii) gas mixture temperature (mixture of water vapor and non-condensable gas), and (iii) partial pressure of the non-condensable gas. If P_{nc} remains constant with increasing P_{tot}, P_v increases, and the condensation rate increases owing to the higher diffusion rate caused by the high density of water molecules. In addition, because the inside of the vessel remains saturated, T_{sat} increases with increasing P_v; thus, the diffusion of the non-condensable gas–water vapor mixture is accelerated according to the Chapman–Enskog theory [60]. By contrast, when P_{nc} increases at a constant P_v, more non-condensable gas molecules act as a barrier that prevents the diffusion of water vapor molecules to the wall. Because Fig. 3(c) shows that the average heat transfer coefficients increase with increasing P_{tot} at a constant W_{nc}/(1-W_{nc}), the effects of (i) P_v and (ii) T_{sat} on the condensation heat transfer process are greater than that of (iii) P_{nc}. Therefore, empirical correlations for the condensation heat transfer coefficients are proposed. Eq. (5) presents the proposed condensation heat transfer correlation for the presence of non-condensable gases:

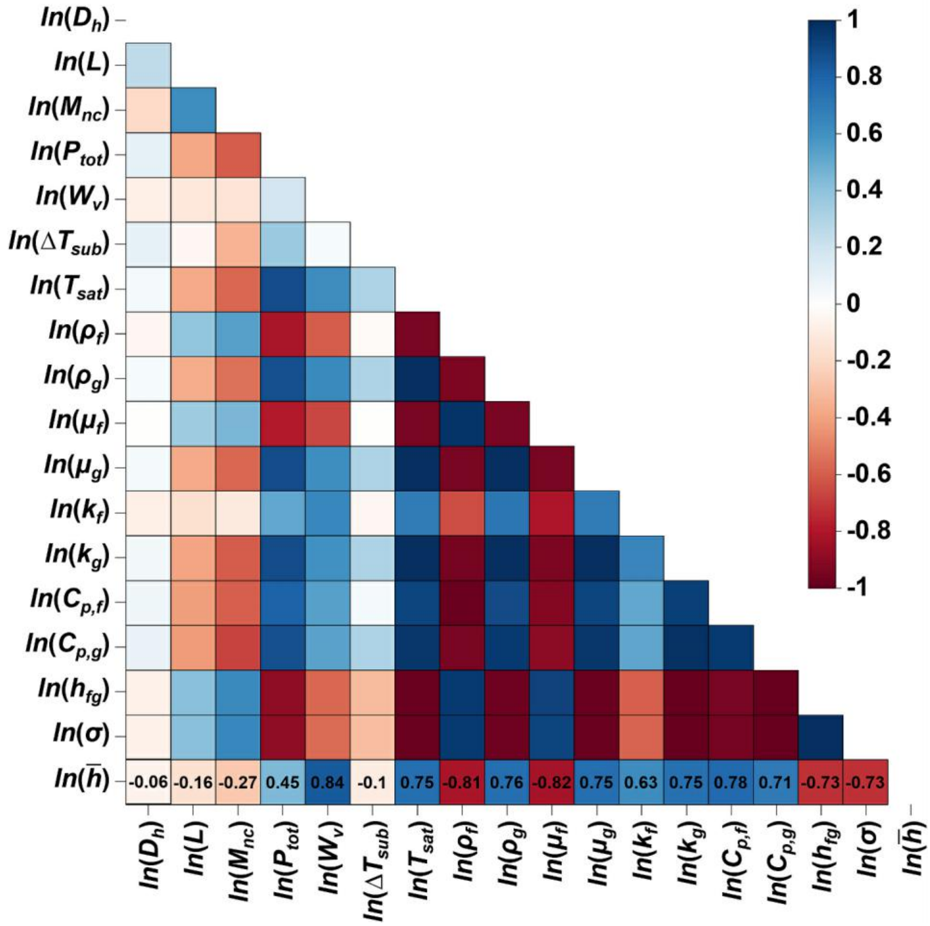

Fig. 4. Pearson correlation coefficients with respect to input parameters for the multilayer perceptron (MLP) neural network.

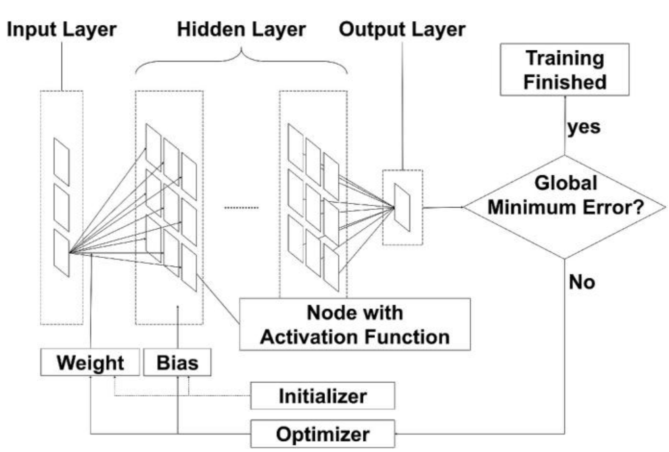

Fig. 5. Architecture of the multilayer perceptron (MLP) neural network.

$$\bar{h} = C_1\left(\frac{L}{D_h}\right)^{C_2}\left(\frac{W_{nc}}{1-W_{nc}}\right)^{C_3}(P_v)^{C_4}(\Delta T_{sub})^{C_5} \tag{5}$$

where L/D_h accounts for the turbulent effect of the liquid film along the tube length and the effect of the tube curvature [22,61]; C_1–C_5 in Eq. (5) were determined with the generalized reduced gradient (GRG) nonlinear algorithm [62]; the final values were optimized to $C_1 = 3.18$, $C_2 = 0.1$, $C_3 = -0.47$, $C_4 = 0.51$, and $C_5 = -0.34$. However, this correlation caused the heat transfer coefficient to approach infinity for a very small or zero non-condensable gas mass fraction. Thus, we proposed a correlation below:

$$\bar{h} = \bar{h}_{plate}\left(\frac{L}{D_h}\right)^{C_6}\exp\left[C_7\left(\frac{W_{nc}}{1-W_{nc}}\right)^{C_8}\left(\frac{P_{tot}}{P_c}\right)^{C_9}\right] \tag{6}$$

where $\bar{h}_{plate}$ is the condensation heat transfer coefficient on a flat plate [16]:

$$\bar{h}_{plate} = 1.01Re_{film}^{-0.22}k_f\left(\frac{g}{\nu_f^2}\right)^{1/3} \tag{7}$$

and P_c is the critical pressure of the working fluid ($P_c = 22.064$ MPa for water). All liquid properties were evaluated for the film temperature that was determined based on the wall and saturation temperatures; the vapor properties were evaluated for the saturation temperature corresponding to the partial pressure of the water vapor. In addition, C_6–C_9 were determined to be $C_6 = 0.18$, $C_7 = -1.78$, $C_8 = 0.21$, and $C_9 = -0.11$ with Eq. (6) and the GRG nonlinear algorithm. It should be noted that C_7 is negative to avoid an infinite heat transfer coefficient at $W_{nc} = 0$.

2.2.2. Multilayer perceptron (MLP) model

Before developing the proposed MLP model (a type of artificial neural network), the simple interrelationships between the average heat transfer coefficient and various input parameters were analyzed with the Pearson correlation coefficient, which is referred to as "R" [63]. The Pearson correlation coefficient analysis is a commonly used statistical approach that measures the linear correlation between two variables with R:

Table 3
Mean absolute errors (MAEs) of validation set with respect to numbers of layers and nodes.

Unit [%]	2 layers	4 layers	6 layers	8 layers	10 layers
2 nodes	21.2	21.3	16.0	16.8	21.5
4 nodes	15.0	14.9	11.2	12.5	12.8
6 nodes	21.0	14.3	15.6	14.0	13.6
8 nodes	22.0	8.6	13.3	14.2	13.7
10 nodes	12.5	9.4	15.4	10.3	12.5
12 nodes	11.3	8.2	8.1	9.4	8.4
14 nodes	14.4	6.4	8.4	6.4	12.1
16 nodes	8.7	13.0	7.8	8.3	13.1
18 nodes	13.9	7.6	6.2	12.3	9.7
20 nodes	8.0	10.3	6.2	7.7	8.3
22 nodes	13.2	6.2	5.8	7.1	9.2
24 nodes	7.4	7.1	7.9	12.5	9.5
26 nodes	6.9	6.2	5.6	7.1	7.4
28 nodes	6.6	6.2	7.0	7.7	7.5
30 nodes	7.1	13.4	8.2	12.4	13.0
32 nodes	6.0	10.9	6.8	6.4	12.2
34 nodes	5.8	7.2	9.3	10.6	10.8
36 nodes	6.7	6.7	6.8	7.6	11.8
38 nodes	5.9	7.9	6.0	10.4	7.7
40 nodes	6.5	6.7	6.1	9.7	12.3

$$R_{AB} = \frac{\sum_i^n \left(A_i - \overline{A}\right)\left(B_i - \overline{B}\right)}{\sqrt{\sum_i^n \left(A_i - \overline{A}\right)^2}\sqrt{\sum_i^n \left(B_i - \overline{B}\right)^2}} \tag{8}$$

where R has a value between +1 and −1, which indicate a total positive and total negative linear relationship, respectively. The greater the absolute value of R is, the stronger is the relationship between the two variables. As shown in Fig. 4, the absolute values of R for D_h, L, M_{nc}, and ΔT_{sub} are <0.3; thus, the relationship with the heat transfer coefficients is relatively weak while $|R| > 0.8$ for W_v. Most properties show significant correlations with the heat transfer coefficients because the properties strongly depend on the partial pressure of the water vapor, which is determined by P_{tot} and W_v.

In this study, Python (Version 3.6) and TensorFlow (Version 1.13.1) were used to implement the MLP model, which was trained to predict the condensation heat transfer coefficients. Fig. 5 shows the architecture of the proposed MLP model, which consists of input and output layers and hidden layers; the hidden layers include nodes with activation functions, initializer, optimizer, weights, and biases. The input layer accepts a natural logarithm form with geometrical and operating conditions and the properties of the three different phases (water vapor, water liquid, and non-condensable gas): L, D_h, P_{tot}, ΔT_{sub}, W_{nc}, T_{sat}, ρ_f, ρ_g, μ_f, μ_g, k_f, k_g, $C_{p,f}$, $C_{p,g}$, h_{fg}, σ, and M_{nc}. Each node in the hidden layers is determined by its weight, bias, and activation function:

$$\psi_{i,j} = f\left(b_{i,j} + \sum_{j=1}^{n} w_{i,j}\psi_{i-1,j}\right) \tag{9}$$

where $\psi_{i,j}$ is the node value of the j-th node in the i-th layer, and f, b, and w are the activation function, bias, and weight of the associated node, respectively. Moreover, a Leaky Rectified Linear Unit (LReLU) [64] was used as the activation function, which can be expressed as follows:

$$f(x) = \begin{cases} x & x \geq 0 \\ 0.2x \; for \; x < 0 \end{cases} \tag{10}$$

where 0.2 is the coefficient of the negative values used to avoid zero. The weights and biases were initialized following the work of He *et al.* [65]; their initialization approach resulted in better convergence with several variants of the Rectified Linear Unit (ReLU) such as the LReLU.

and Parametric ReLu (PReLU). More specifically, the weights were initialized at the beginning of the training such that the following expression holds [65]:

$$\frac{1}{n} n_i Var[w_i] = 1, \quad \forall i \tag{11}$$

where $Var[w_i]$ represents the variance of the weights in each layer i with n_i nodes. The biases were initialized to zero [65]. The predicted heat transfer coefficients were determined at the end of the output layer and compared to the experimentally determined average heat transfer coefficients. Subsequently, the weights and biases were updated by an Adam optimizer [66], which is a widely used optimizer for ANN models, to reduce the error with a 0.005 learning rate.

The consolidated database was classified into training, validation, and test datasets, which comprised 80 %, 10 %, and 10 % of the total data points, respectively. The training and validation datasets were used to optimize the numbers of layers and nodes, and the test dataset was used to report the final results. The network was trained with 30,000 epochs, while an early stopping was activated after 2000 epochs to avoid overfitting. The model selection of the MLP architecture was conducted with 2–10 testing layers with 2–40 nodes for each hidden layer. In total, 100 combinations of hyperparameters were tested with the same training dataset and conditions. Table 3 provides the MAEs of the validation dataset with respect to the numbers of layers and nodes. The MAE can be determined as follows:

Table 5a
Summary of solution models and parameters.

Solution models	
Machine learning model	Multilayer perceptron (MLP)
Tool	Python (Version 3.6) and TensorFlow (Version 1.13.1)
Input	Natural logarithm of L, D_h, P_{tot}, ΔT_{sub}, W_{nc}, T_{sat}, ρ_f, ρ_g, μ_f, μ_g, k_f, k_g, $C_{p,f}$, $C_{p,g}$, h_{fg}, σ, and M_{nc}
Output	Average heat transfer coefficient
Activation function	Leaky Rectified Linear Unit (LReLU) [64]
Initializer	He initializer [65]
Optimizer	Adam optimizer [66]
Learning rate	0.005
Hyperparameter optimization	
Layers	2–10 layers
Nodes	2–40 nodes
Maximum training	30,000 epochs
Early stopping	2000 epochs
Training dataset validation	
Layers	6 layers
Nodes	26 nodes
Maximum training	50,000 epochs
Early stopping	5000 epochs

Table 4
Results of generalization of training dataset.

MAE	Case1	Case2	Case3	Case4	Case5	Case6	Case7	Case8	Case9
Training dataset [%]	4.9	5.3	6.5	5.8	3.9	4.5	4.9	6.3	6.1
Validation dataset [%]	6.7	5.0	6.8	7.6	5.2	7.3	7.4	6.2	5.3
Test dataset [%]	6.4	7.4	7.7	6.8	6.0	6.8	6.4	6.9	7.3
Total [%]	5.2	5.5	6.7	6.1	4.2	5.0	5.3	6.4	6.1

Table 5b
Relevant correlations and proposed regression model for water vapor free-falling condensation with non-condensable gases.

Author(s)	Correlation	Geometry	Range
Geometry–independent correlation			
Uchida *et al.* (1965) [57]	$\overline{h} = 380\left(\frac{1-W_{nc}}{W_{nc}}\right)^{0.7}$	Plate	$0.23 \le W_{nc} \le 0.91$
Kataoka *et al.* (1992) [58]	$\overline{h} = 430\left(\frac{1-W_{nc}}{W_{nc}}\right)^{0.8}$	Plate	$0.5 \le W_{nc} \le 0.91$
Murase *et al.* (1993) [59]	$\overline{h} = 470\left(\frac{1-W_{nc}}{W_{nc}}\right)$	Plate	$0.46 \le W_{nc} \le 0.98$
Liu *et al.* (2000) [23]	$\overline{h} = 55.635X_v^{2.344}P_{tot}{}^{0.252}\Delta T_{sub}^{0.307},\ X_v = \frac{W_v/M_v}{W_v/M_v + W_{nc}/M_{nc}}$	Circular tube	$0.25 \le P_{tot} \le 0.46$ MPa $4 \le \Delta T_{sub} \le 25$ K $0.1 \le W_{nc} \le 0.7$
Ahn (2007) [24]	$\overline{h} = [(371.41 - 36.5P_{tot}) + (695.63 - 261.52P_{tot})\log_{10}(W_{nc})]\Delta T_{sub}^{0.25}$	Circular tube	$0.4 \le P_{tot} \le 1.2$ MPa $30 \le \Delta T_{sub} \le 50$ K $0.2 \le W_{nc} \le 0.8$
Su *et al.* (2013) [27]	$\overline{h} = [10189.3 + 90416.4P_{tot} - (4314.4 + 46537P_{tot})\log_{10}(100W_{nc})]\Delta T_{sub}^{-0.6}$	Circular tube	$0.2 \le P_{tot} \le 0.6$ MPa $27 \le \Delta T_{sub} \le 70$ K $0.2 \le W_{nc} \le 0.8$
Su *et al.* (2014) [28]	$\overline{h} = [-2913.62 + 7957.3P_{tot} - (7841.62 + 3051.85P_{tot})\log_{10}W_{nc}]\Delta T_{sub}^{-0.35}$	Circular tube	$0.4 \le P_{tot} \le 0.6$ MPa $13 \le \Delta T_{sub} \le 25$ K $0.07 \le W_{nc} \le 0.52$
Fan *et al.* (2018b) [33]	$\overline{h} = \frac{[(32021 - 22766P_{tot}) + (-16107 + 11736P_{tot})\log_{10}(100W_{nc})]}{\Delta T_{sub}^{(0.561+0.00134\Delta T_{sub}-0.546P_{tot})}}$	Circular tube	$0.2 \le P_{tot} \le 0.5$ MPa $10 \le \Delta T_{sub} \le 70$ K $0.1 \le W_{nc} \le 0.8$
Geometry–dependent correlation			
Dehbi (1991) [22]	$\overline{h}_{plate} = \frac{L^{0.05}[(3.7 + 28.7P_{tot}) - (2438 + 458.3P_{tot})\log_{10}W_{nc}]}{\Delta T_{sub}^{0.25}},\ \overline{h}_{tube} = 1.25\overline{h}_{plate}$	Circular tube	$0.3 \le L \le 3.5$ m $0.15 \le P_{tot} \le 0.46$ MPa $10 \le \Delta T_{sub} \le 50$ K $0.25 \le W_{nc} \le 0.91$
	$\overline{h}_{plate} = 0.185D_{AB}^{2/3}(\rho_w + \rho_\infty)\left(\frac{\rho_w - \rho_\infty}{\mu_{eff}}\right)^{1/3}\frac{h_{fg}}{\Delta T_{sub}}\ln\left(\frac{1-W_{v,w}}{1-W_{v,\infty}}\right),\ D_{AB} = \frac{10^{-3}T_f{}^{1.5}\left[3.03 - \left(\frac{0.98}{M_{AB}^{0.5}}\right)\right]}{P_{tot}M_{AB}^{0.5}d_{AB}^2\Omega_D},$ $\mu_{eff} = \sum_{i=1}^{2}\frac{X_i\mu_i}{\sum_{j=1}^{2}X_j\Phi_{ij}},\ M_{AB} = \left(\frac{1}{M_A} + \frac{1}{M_B}\right)^{-1},\ d_{AB} = 0.5(d_A + d_B),\ \Phi_{ij} = \frac{[1 + (\mu_i/\mu_j)^{0.5}(M_j/M_i)^{0.25}]^2}{[8(1 + M_i/M_j)]^{0.5}},$ $\Omega_D = \frac{\alpha_1}{(T^*)^{\alpha_2}} + \frac{\alpha_3}{e^{\alpha_4 T^*}} + \frac{\alpha_5}{e^{\alpha_6 T^*}} + \frac{\alpha_7}{e^{\alpha_8 T^*}},\ \alpha_1 = 1.06036,\ \alpha_2 = 0.1561,\ \alpha_3 = 0.1930,\ \alpha_4 = 0.47635,\ \alpha_5 = 1.03587,\ \alpha_6 = 1.52996,$ $\alpha_7 = 1.76474,\ \alpha_8 = 3.89411,\ T^* = \frac{T_f}{(\varepsilon_{AB}/\kappa)},\ \frac{\varepsilon_{AB}}{\kappa} = \left(\frac{\varepsilon_A}{\kappa}\frac{\varepsilon_B}{\kappa}\right)^{0.5},\ \frac{\overline{h}_{tube}}{\overline{h}_{plate}} = 1 + 0.3\left(\sqrt{32}\,Gr_L^{-1/4}\frac{L}{D_h}\right)^{0.909},\ Gr_L = \frac{g\beta(T_w - T_\infty)L^3}{\nu^2}$	Circular tube	$0.1 \le P_{tot} \le 2.0$ MPa $4 \le \Delta T_{sub} \le 140$ K $0.09 \le W_{nc} \le 0.94$
Lee *et al.* (2017) [30]	$\overline{h} = 890Gr_L^{0.125}W_v^{*0.966}Ja^{-0.327}\frac{k_{eff}}{D_h},\ k_{eff} = \sum_{i=1}^{2}\frac{X_i k_i}{\sum_{j=1}^{2}X_j\Phi_{ij}},\ \Phi_{ij} = \frac{[1 + (k_i/k_j)^{0.5}(M_j/M_i)^{0.25}]^2}{[8(1 + M_i/M_j)]^{0.5}},$ $W_v^* = 1 - W_{nc}^{0.01},\ Gr_L = \frac{g\rho(\rho_w - \rho_\infty)L^3}{\mu_{eff}{}^2},\ \mu_{eff} = \sum_{i=1}^{2}\frac{X_i\mu_i}{\sum_{j=1}^{2}X_j\Phi_{ij}},\ X_i = \frac{W_i/M_i}{W_i/M_i + W_j/M_j},$ $Ja = \frac{C_{p,eff}(T_\infty - T_w)}{h_{fg}},\ C_{p,eff} = W_v C_{p,v} + W_{nc}C_{p,nc}$	Circular tube	$1 \le L \le 3.5$ m $1.36 \times 10^{10} \le Gr_L \le 5.05 \times 10^{12}$ $0.009 \le Ja \le 0.035$ $1.16 \times 10^{-3} \le W_v{}^* \le 2.35 \times 10^{-2}$
Jang *et al.* (2018) [31]	$\overline{h} = 0.165h_{nu}\exp(-1.852W_{nc})\left(\frac{L}{D_h}\right)^{0.529}\left(\frac{P_v}{P_c}\right)^{0.36}\left(\frac{\Delta T_{sub}}{T_c}\right)^{-0.219}$	Circular tube	$25 \le L/D_h \le 100$ $0.025 \le P_v \le 0.47$ MPa $18 \le \Delta T_{sub} \le 69$ K $0.1 \le W_{nc} \le 0.89$
Proposed regression model	$\overline{h} = 3.18\left(\frac{L}{D_h}\right)^{0.1}\left(\frac{W_{nc}}{1-W_{nc}}\right)^{-0.47}(P_v)^{0.51}(\Delta T_{sub})^{-0.34}$	Circular tube	$15 \le L/D_h \le 100$ $0.02 \le P_v \le 1.92$ MPa $5 \le \Delta T_{sub} \le 71$ K $0.01 \le W_{nc} \le 0.9$

$$\mathrm{MAE} = \frac{1}{N}\sum\frac{\left|\overline{h}_{\exp} - \overline{h}_{pred}\right|}{\overline{h}_{\exp}} \times 100\% \tag{12}$$

As indicated in Table 3, the MAEs decrease with the number of nodes. In addition, the MAEs decrease as the number of layers increases to six. The best result is achieved for a combination of six layers and 26 nodes with an MAE of 5.6 %. Subsequently, the training and validation datasets were classified into nine datasets with equivalent sizes; each dataset was evaluated with a network trained on the remaining eight datasets to improve the accuracy and generalize the training dataset. The networks were trained with 50,000 epochs with an early stopping after 5000 epochs. Table 4 provides the MAEs of the nine different training datasets of the training, validation, and test datasets. The differences in the MAEs of all datasets are within 1.7 %–2.6 %; the best results exhibit MAEs of 3.9 %, 5.2 %, and 6.0 % for the training, validation, and test datasets, respectively.

3. Results and discussion

3.1. Evaluation of relevant correlations

The accuracies of 12 relevant correlations were assessed by comparing their MAEs (Eq. (12)). Furthermore, two additional parameters (θ and ξ) were used to evaluate the accuracies; they indicate the percentages of predicted data points with MAEs within ±30 % and ±50 %, respectively.

Table 5 summarizes the relevant correlations and their applicable ranges reported in literature. The correlations are categorized into two groups: those with and without geometrical conditions. The first group

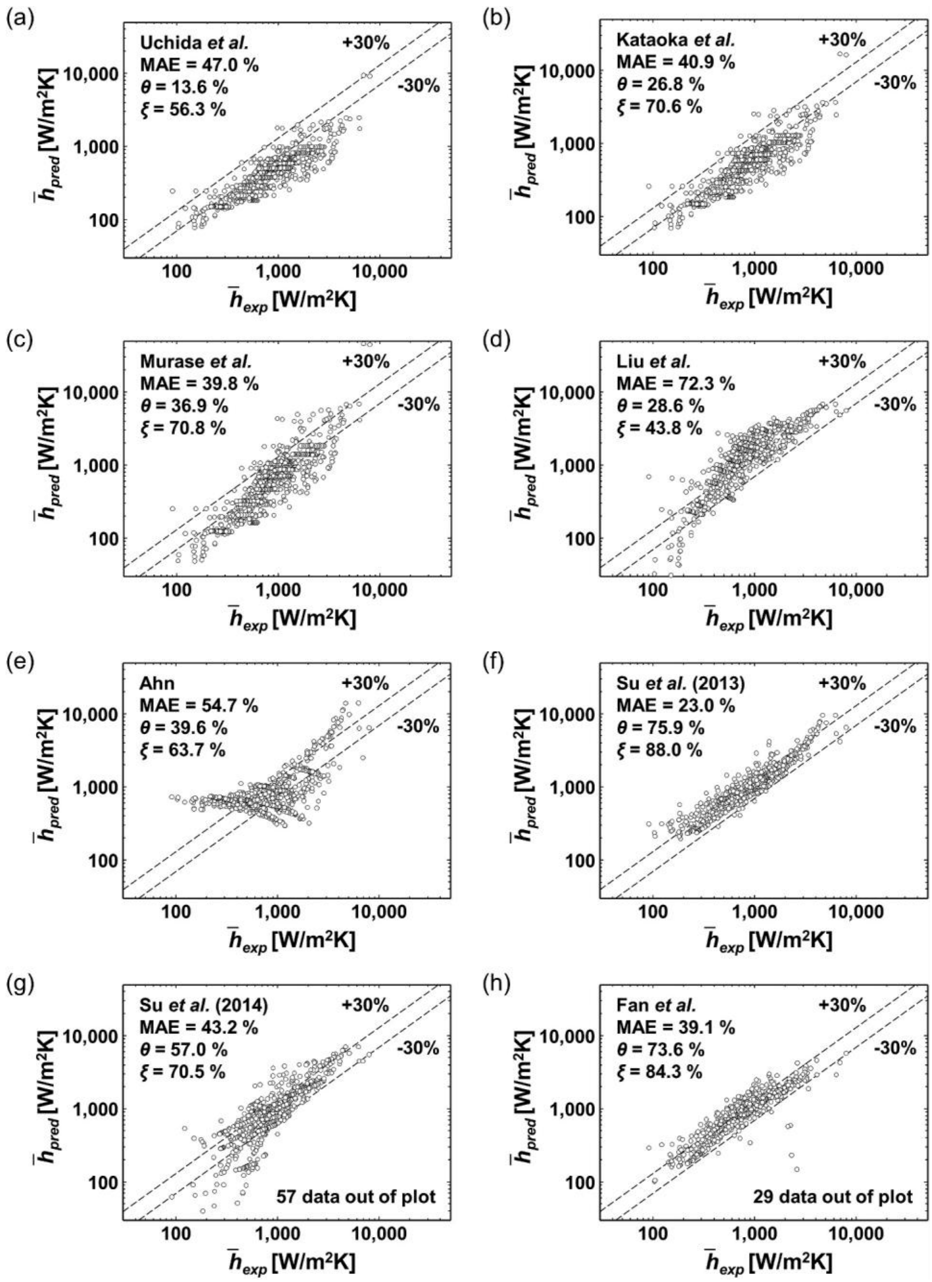

Fig. 6. Comparison of the consolidated experimental database with predictions by using the first group of correlations: (a) Uchida *et al.* [57], (b) Kataoka *et al.* [58], (c) Murase *et al.* [59], (d) Liu *et al.* [23], (e) Ahn [24], (f) Su *et al.* (2013) [27], (g) Su *et al.* (2014) [28], (h) Fan *et al.* [33]. $\bar{h}_{exp}$, average expected condensation heat transfer coefficient; $\bar{h}_{pred}$, average predicted condensation heat transfer coefficient; MAE, mean absolute error; θ, percentage of data with MAE within $\pm$30 %; ξ, percentage of data with MAE within $\pm$50 %.

of correlations was developed without considering the geometrical parameters. Uchida *et al.* [57] experimentally determined the heat transfer coefficients on a vertical plate for a wide range of W_{nc} (0.23–0.91). The correlation determined by fitting their data is the most widely used for predicting the condensation heat transfer coefficients in non-condensable gas owing to its ease of use. However, Peterson [67] indicated that the correlation of Uchida *et al.* [57] is unsuitable for a plate with a length of longer than 0.3 m owing to the absence of geometrical terms. In addition, he theoretically demonstrated that the correlation of Uchida *et al.* [57] underpredicts the heat transfer rate in the range of $P_{nc} > 1.0$ bar and overpredicts it in the range of $P_{nc} < 1.0$ bar. Kataoka *et al.* [58] and Murase *et al.* [59] modified the constants in the correlation of Uchida *et al.* based on the reported experimental data for a wider W_{nc} range (0.46–0.98). Although Uchida *et al.* [57] developed the correlation for vertical plates, the correlation provides good predictions for vertical tubes [30]. Liu *et al.* [23] proposed a correlation including water vapor mole fraction, total pressure and wall subcooling temperature. The correlations proposed by Ahn [24], Su *et al.* [27], and Fan *et al.* [33] were developed based on similar expressions for the total pressure, mass fraction of the non-condensable gas, and wall subcooling temperature; however, the geometrical parameters were not considered.

The second group consists of correlations developed based on geometrical and operating conditions. Dehbi [22] developed a correlation based on 216 experimental data points; the tube length was included in the correlation to consider the effect of the film thickness and turbulence on the condensed liquid film. Later, the researchers proposed a new correlation [68], which included the diameter, length, diffusion coefficient, density, and enthalpy based on a consolidated dataset consisting of 350 data points from six sources. Moreover, Lee *et al.* [30] and Jang *et al.* [31] proposed correlations that consider the tube diameter and length. The correlation proposed by Jang *et al.* [31] is based on the heat transfer coefficient from Nusselt's theory [11]; it adopts the geometrical configurations and operating conditions such as the tube length, tube diameter, mass fraction of the non-condensable

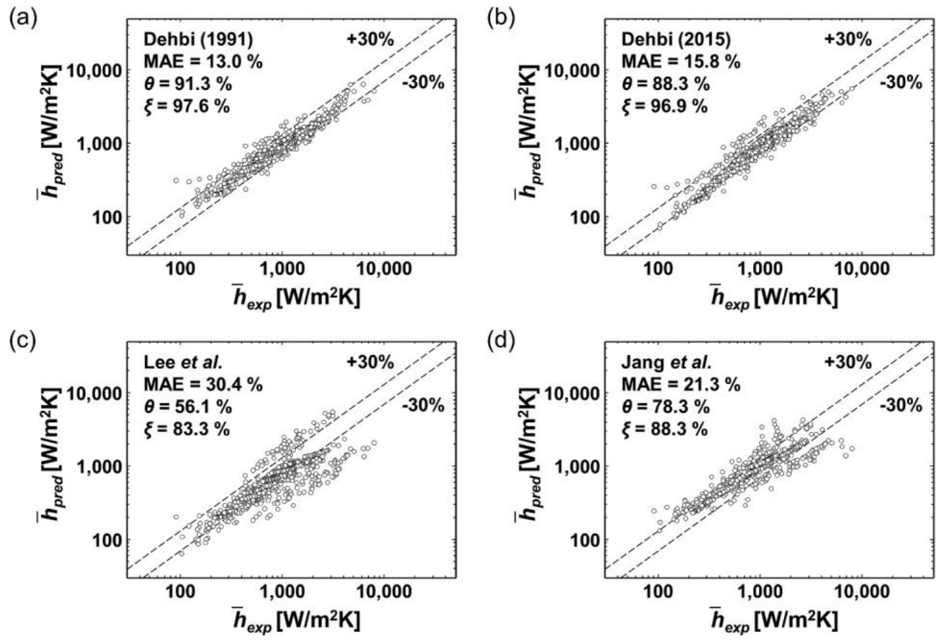

Fig. 7. Comparison of the consolidated experimental database with predictions by using correlations from the second group: (a) Dehbi (1991) [22], (b) Dehbi (2015) [68], (c) Lee *et al.* [30], and (d) Jang *et al.* [31].$\bar{h}_{exp}$, average expected condensation heat transfer coefficient; $\bar{h}_{pred}$, average predicted condensation heat transfer coefficient; MAE, mean absolute error; θ, percentage of data with MAE within ±30 %; ξ, percentage of data with MAE within ±50 %.

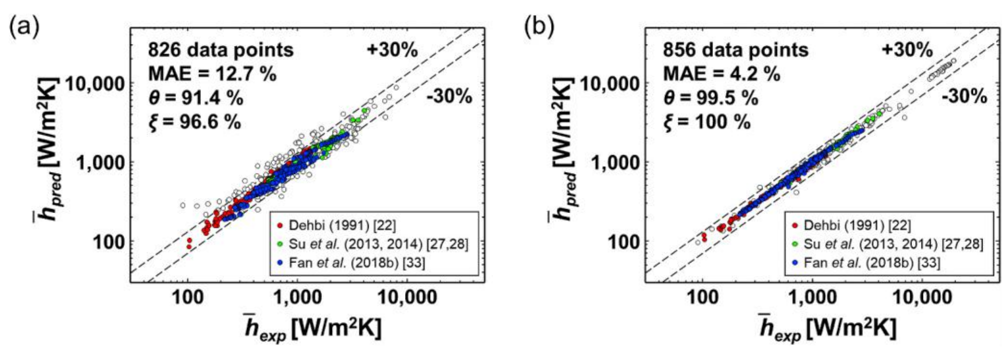

Fig. 8. Comparison of the predictions by using the proposed prediction methods and the consolidated database: (a) the nonlinear regression model and (b) the multilayer perceptron (MLP) neural network model.$\bar{h}_{exp}$, average expected condensation heat transfer coefficient; $\bar{h}_{pred}$, average predicted condensation heat transfer coefficient; MAE, mean absolute error; θ, percentage of data with MAE within ±30 %; ξ, percentage of data with MAE within ±50 %.

gas, partial pressure of the water vapor, and wall subcooling temperature.

Fig. 6 compares the predictions of the first group of correlations in Table 5 against the consolidated database. It should be noted that the compared data points represent the condensation heat transfer on the external surface of vertical circular tubes in the presence of non-condensable gas; the 30 data points representing the pure-water vapor conditions are excluded. As shown in Fig. 6(a), the correlation of Uchida *et al.* [57] provides poor predictions with an MAE of 47.0 % and underpredicts most of the data; 112 and 465 data points out of 826 data points have MAEs within ±30 % and ±50 % ($\theta = 13.6$ %, $\xi = 56.3$ %, respectively). The correlations of Kataoka *et al.* [58] and Murase *et al.* [59] (in Fig. 6(b) and (c)) show very similar trends to that of Uchida *et al.*; however, the predictions are slightly better, with MAEs of 40.9 % and 39.8 %, respectively. Both correlations underpredict most of the data points, such as the correlation of Uchida *et al.* [57]. In addition, the correlation of Liu *et al.* [23] exhibits poor predictions and substantially overpredicts $\bar{h}$ against the database with an MAE of 72.3 %, $\theta = 28.6$ %, and $\xi = 43.8$ %. The correlations of Ahn [24] and Su *et al.* (2013, 2014) [27] [28] have similar expressions. The correlation of Su *et al.* (2013) [27] results in excellent predictions with an MAE of 23.0 %, $\theta = 75.9$ %, and $\xi = 88.0$ %; the other two correlations provide relatively poor predictions with MAEs of 54.7 % (Ahn) and 43.2 % (Su *et al.* (2014)). Moreover, the correlation of Su *et al.* (2014) [28] exhibits particularly poor predictions for low $\bar{h}_{exp}$ values because the application range of the subcooling temperature is narrow. It should be noted that 57 out-of-range data points (including 52 data points with negative $\bar{h}_{\mathrm{pred}}$) are not marked in Fig. 6(g). Fig. 6(h) shows the results predicted with the correlation of Fan *et al.* [33], which shows fair predictions with an MAE of 39.1 %, $\theta = 73.6$ %, and $\xi = 84.3$ % for 29 out-of-range data points with 27 negative $\bar{h}$ data points in the range of $P_{tot} \geq 1.5$ MPa. Overall, most of the correlations from the first group provide poor predictions because they cannot accommodate heat transfer changes with geometrical variations.

Fig. 7(a–d) presents the predictions of the correlations from the second group, which consider geometry-dependent parameters. The two correlations proposed by Dehbi [22,68] show good predictions with MAEs of 13.0 % and 15.8 %, respectively. The first correlation [22] provides the best predictions among the relevant correlations (with an MAE of 13.0 %, $\theta = 91.3$ %, and $\xi = 97.6$ %). The correlation proposed by Lee *et al.* [30] shows fair predictions with an MAE of 30.4 %, which is relatively high compared to those of the other correlations in the second

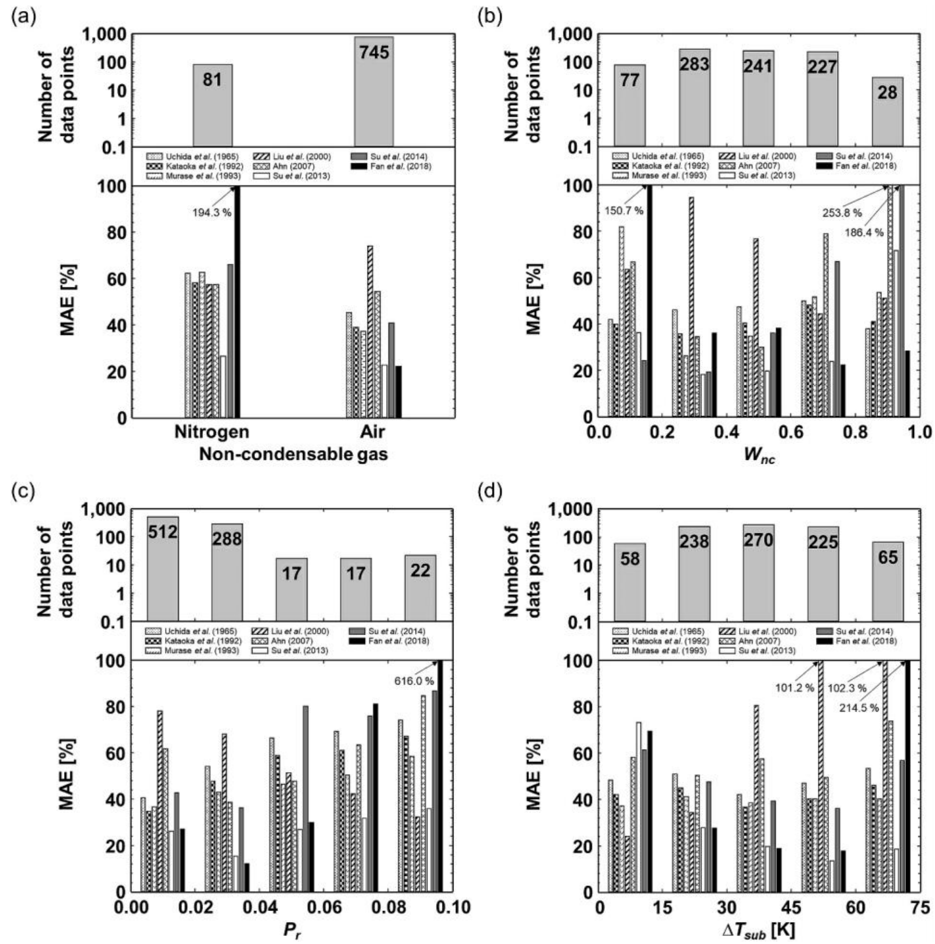

Fig. 9. Mean absolute error (MAE) distributions of predictions of first group of correlations for the consolidated database with respect to (a) types of non-condensable gas, (b) mass fraction of non-condensable gas (W_{nc}), (c) reduced pressure (P_r), and (d) wall subcooling temperature (ΔT_{sub}).

group; the main reason is the lower prediction accuracy for $L < 1$ m. The correlation of Jang *et al.* [31] provides good predictions with an MAE of 21.3 %, $\theta = 78.3$ %, and $\xi = 88.3$ %. Overall, the correlations in this group provide much better predictions than those of the first group.

3.2. Proposed prediction methods

Furthermore, the predictions of the proposed methods based on (1) nonlinear regression and (2) MLP models were compared. Fig. 8(a) shows the predictions of the regression model; the results for the consolidated database are excellent; the MAE is 12.7 % with $\theta = 91.4$ % and $\xi = 96.6$ % (Eq. (5)). The data from Dehbi [22], Su *et al.* (2013, 2014) [27], [28] and Fan *et al.* [33] account for 25.2 %, 17.5 % and 24.8 % of the consolidated database, respectively. Evidently, the new regression model provides the best results among all methods listed in Table 5. The available correlation for $W_v = 1$ (Eq. (6)) exhibits a good accuracy with an MAE of 14.9 %, $\theta = 87.1$ %, and $\xi = 96.6$ %.

Fig. 8(b) shows the predictions of the MLP of case 5 in Table 4. It should be noted that the 30 pure-water vapor data points are included such that the network can be trained on very low non-condensable gas cases. As shown in Fig. 8(b), the MLP model shows a superior prediction accuracy for the consolidated database with an overall MAE of 4.2 %, which is a more than three-fold reduction in the MAE; 99.5 % and 100 % of the 856 consolidated data points have MAEs within ±30 % and ±50 %, respectively.

Figs. 9–13 compare the accuracies of the relevant correlations and proposed models with respect to the geometrical and operation ranges. More specifically, Fig. 9 compares the MAEs of the first group of correlations according to the different ranges of the operating conditions. As shown in Fig. 9(a), the correlations in this group exhibit better predictions for air than for nitrogen because most nitrogen data are biased for high P_{tot} and ΔT_{sub} values. The correlation of Su *et al.* (2013) [27] shows good predictions for nitrogen data for high ΔT_{sub} values. The correlation of Fan *et al.* [33] exhibits the most inaccurate results with an MAE of 194.3 % for the nitrogen data. Moreover, Fig. 9(b) shows the prediction accuracies for the mass fraction of the non-condensable gas (W_{nc}). The correlation of Fan *et al.* [33] shows poor predictions for $W_{nc} < 0.2$ with an MAE of 150.7 %. The correlations of Ahn [24] and Su *et al.* (2014) [28] provide inferior prediction accuracies for $W_{nc} \geq 0.8$ with MAEs of 253.8 % and 186.4 %, respectively, whereas the correlation of Su *et al.* (2013) [27] shows the best predictions for the intermediate range of the mass fraction of the non-condensable gas ($W_{nc} = 0.2$–0.8). Furthermore, Fig. 9(c) compares the prediction accuracies with respect to the reduced total pressure P_r, which is determined by P_{tot}/P_c. The MAEs tend to increase with increasing P_r for most correlations because they were developed based on data with $P_r < 0.06$. The correlations of Su *et al.* (2013) [27] and Fan *et al.* [33] show the best accuracies for relatively low P_r values, and that of Liu *et al.* [23] exhibits the best accuracy for high P_r values ($P_r \geq 0.06$). Fig. 9(d) presents the prediction accuracies of the first group of correlations with respect to the subcooling temperature. The MAE of the correlation of Liu *et al.* [23] increases with increasing ΔT_{sub} because the correlation is based on relatively low ΔT_{sub} values ($4 \leq \Delta T_{sub} < 25$ K). Such as for the other operating conditions, the correlation of Su *et al.* (2013) [27] shows the best predictions for most subcooling temperature ranges except for $\Delta T_{sub} < 15$ K.

Fig. 10 compares the predictions of the second group of correlations

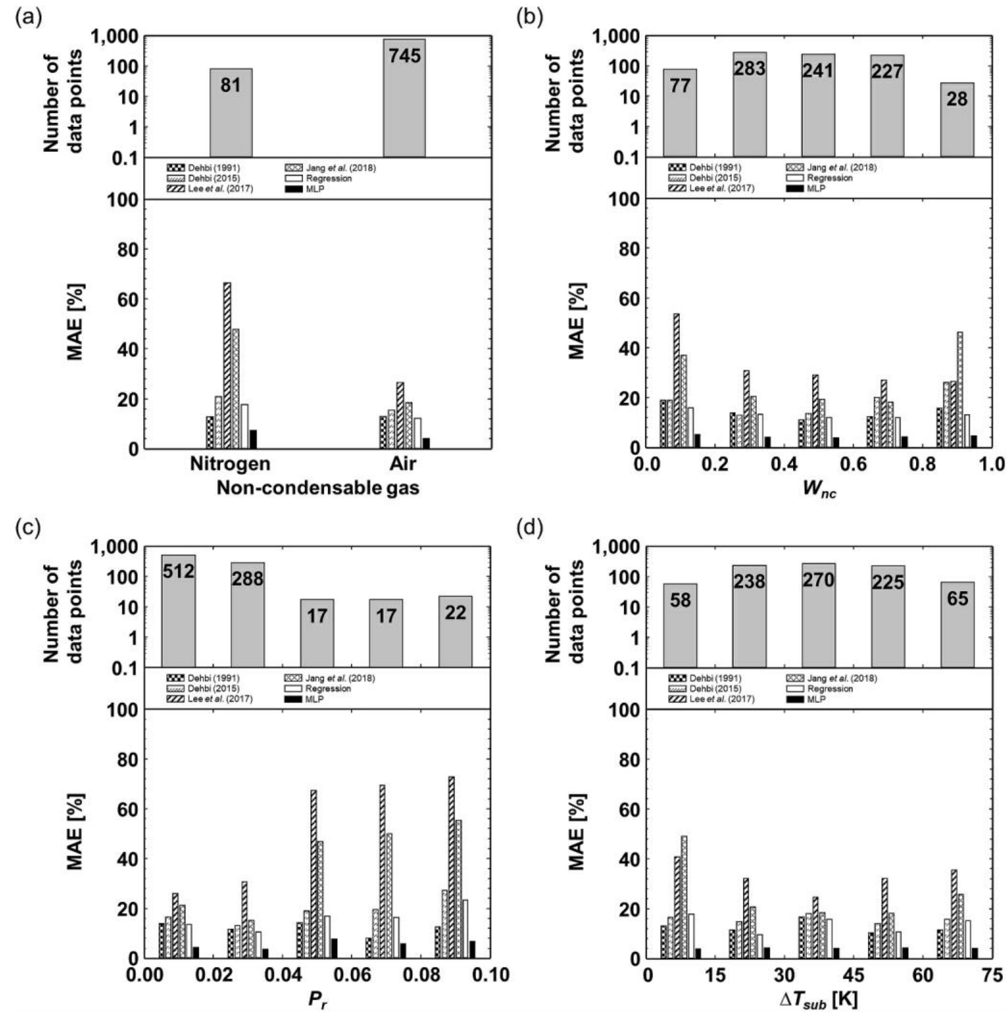

Fig. 10. Mean absolute error (MAE) distributions of predictions of second group of correlations and proposed models for consolidated database with respect to: (a) types of non-condensable gas, (b) mass fraction of non-condensable gas, (c) reduced pressure, and (d) wall subcooling temperature.

and two proposed models with respect to the operating conditions. Accordingly, the second group provides much higher accuracies than the first group. The MAEs for the nitrogen data of certain correlations such as those of Lee *et al.* [30] and Jang *et al.* [31] are significantly higher; nevertheless, most correlations in the second group show relatively small deviations for the non-condensable gas. The proposed regression model provides relatively poor predictions for the nitrogen data compared to that of Dehbi (1991) [22]; however, the predictions for the air data are slightly better. In addition, the MLP model exhibits superior predictions for both non-condensable gases (with MAEs of 7.2 % for nitrogen and 4.0 % for air). Fig. 10(b) shows the prediction difference relative to W_{nc}. All correlations provide good predictions for all W_{nc} ranges, whereas the correlations of Lee *et al.* [30] and Jang *et al.* [31] result in poor predictions for $W_{nc} < 0.2$ and $W_{nc} \geq 0.8$, respectively. In addition, the correlations of Lee *et al.* [30] and Jang *et al.* [31] fail to predict accurately the condensation heat transfer for $P_r \geq 0.04$. The MLP model achieves very low MAEs of 7.6 % for $P_r \geq 0.04$ although a very limited number of data points are available for this range. For $P_r < 0.04$, the proposed regression model shows the best predictions with an MAE of 12.4 % compared to those of the conventional correlations. Furthermore, the MLP model results in even better predictions with an MAE of 4.1 %. Fig. 10(d) presents the results for ΔT_{sub}. The correlation of Jang *et al.* [31], which was developed for the range $18 \leq \Delta T_{sub} \leq 69$ K, provides poor results with an MAE of 49.1 % for the range $\Delta T_{sub} < 15$ K; these are the most inaccurate predictions among those of the correlations of this group. The MLP model exhibits evenly good predictions for all ΔT_{sub} ranges, such as for the other operating conditions.

Fig. 11 (a, c) and (b, d) compare the MAEs of the first and second group of correlations with respect to the geometrical parameters D_h and L. The first group of correlations show high MAEs and deviations for most D_h and L ranges, which is as expected. The correlations of Uchida *et al.* [57], Kataoka *et al.* [58], and Murase *et al.* [59] show similar predictions for most D_h and L ranges. Moreover, the correlations of Liu *et al.* [23], Ahn [24], and Su *et al.* (2014) [28] established for $10 \leq D_h < 20$ mm exhibit the best MAEs (49.0 %, 33.0 %, and 20.5 %, respectively) for all D_h ranges. However, these correlations show poor predictions for data for tubes with large diameters, as demonstrated by the MAEs of 70.2 %, 51.7 %, and 40.7 % for $30 \leq D_h < 40$ mm and MAEs of 91.9 %, 77.6 %, and 64.3 % for $40 \leq D_h < 50$ mm, respectively. Because the correlation of Su *et al.* (2013) [27] was developed based on experimental data for a 2 m long tube, the correlation provides fair MAEs of 10.6 % and 16.0 % for $2 \leq L < 3$ m and $3 \leq L < 4$ m, respectively. However, this correlation provides relatively poor predictions for data from short tubes, as evidenced by the MAEs of 27.9 % for $0 \leq L < 1$ m and 51.0 % for $1 \leq L < 2$ m. The correlation of Fan *et al.* [33] results in good predictions with MAEs of 17.4 % and 9.3 % for narrow geometrical ranges ($30 \leq D_h < 40$ mm and $2 \leq L < 3$ m, respectively). By contrast, the correlation provides the highest MAEs of 140.6 % for $D_h \geq 40$ mm and 167.9 % for $L < 1$ m among the first group of correlations.

The second group of correlations provide much better predictions than the first group (which considers geometrical variations), except those of Lee *et al.* [30] and Jang *et al.* [31]. As shown in Fig. 11(b),

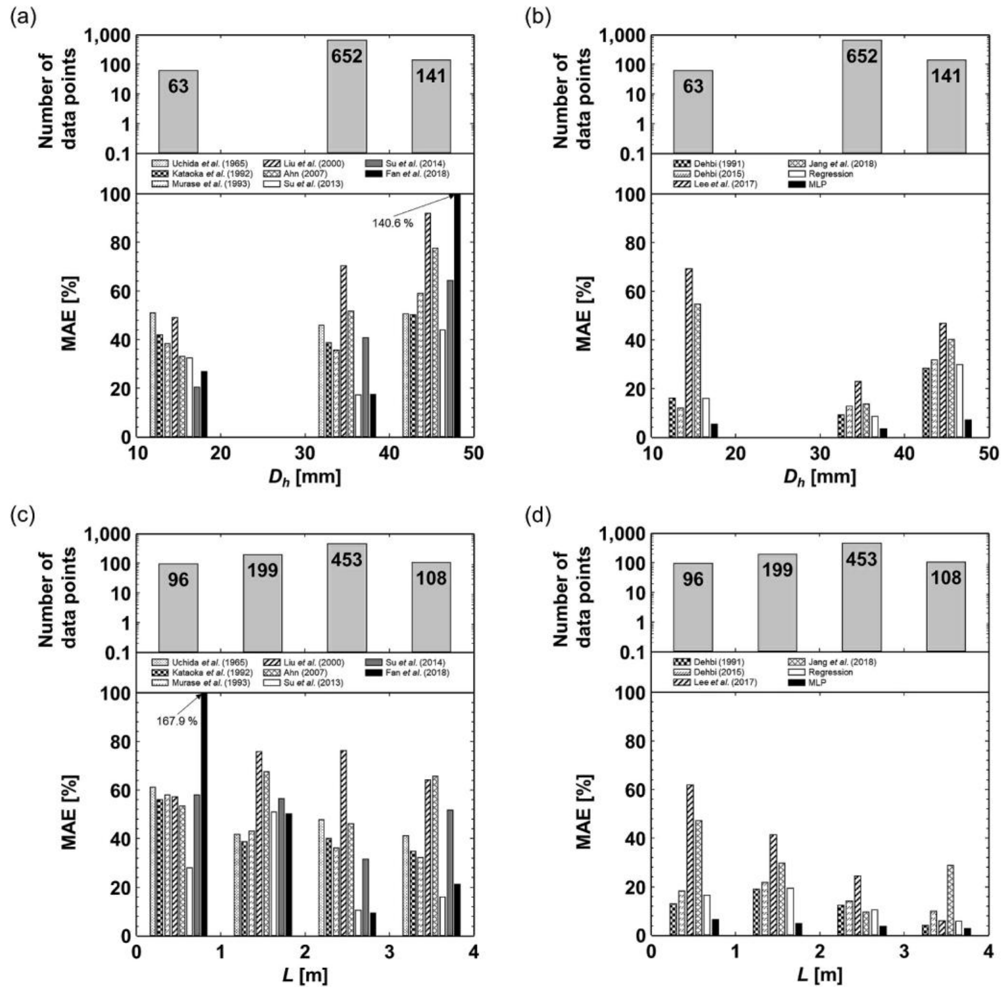

Fig. 11. Mean absolute error (MAE) distributions of predictions of relevant correlations and proposed models for the consolidated database with respect to geometric variations in (a, b) tube hydraulic diameter (D_h) and (c, d) tube length (L).

compared to the conventional correlations, the proposed regression model shows the best predictions with an MAE of 8.5 % for $30 \leq D_h < 40$ mm. For this range, the correlations of Lee *et al.* [30] and Jang *et al.* [31] also show good predictions with MAEs of 22.8 % and 13.6 % and poor MAEs of 69.2 % and 54.8 % for $0 \leq D_h < 10$ mm, respectively. Moreover, the correlations of Dehbi (1991) [22], (2015) [68] and the proposed regression model show the highest MAEs of 28.4 %, 31.6 %, and 29.8 % for large diameters of $40 \leq D_h < 50$ mm, respectively. Fig. 11(d) presents the predictions of the second group of correlations according to the tube length range. The MLP model and all correlations except that of Jang *et al.* [31] show the best predictions for $3 \leq L < 4$ m with MAEs of 4.1 % for Dehbi (1991) [22], 9.8 % for Dehbi (2015) [68], 6.0 % for Lee *et al.* [30], 5.8 % for the proposed regression model, and 2.7 % for the MLP model. Adding geometrical parameters reduces the MAEs for L more effectively than for D_h because the effect of the film thickness and turbulence depending on the tube length is greater than the effect of the changes in the convective heat transfer caused by the tube curvature, as shown in Fig. 4.

Fig. 12 and Fig. 13 compare the MAEs of the first and second group of correlations relative to the (a) average heat transfer coefficient and (b) Reynolds number. In general, the second group predicts the heat transfer coefficients for $\bar{h}$ and Re_{film} more accurately than the first group. As shown in Fig. 12(a and b), the correlation of Su *et al.* (2013) [27] developed for high ΔT_{sub} values provides relatively good predictions for $\bar{h} < 3000$ W/m^2·K and $Re_{film} < 1800$. In addition, the correlation of Su *et al.* (2014) [28] developed for low ΔT_{sub} values provides relatively fair predictions for $\bar{h} \geq 3000$ W/m^2·K and $Re_{film} \geq 1800$. The correlations of Murase *et al.* [59], Ahn [24], and Fan *et al.* [33] show a sharp decrease in accuracy for $\bar{h} \geq 3000$ W/m^2·K, as evidenced by the poorest MAEs of 221.5 %, 120.1 %, and 481.1 % for this range, respectively. Moreover, the correlations of Kataoka *et al.* [58], Murase *et al.* [59], Ahn [24], Su *et al.* (2013) [27], and Fan *et al.* [33] exhibit the worst predictions for $Re_{film} \geq 1800$ with MAEs of 59.5 %, 99.1 %, 105.6 %, 54.1 %, and 538.5 %, respectively.

The correlations of the second group, except those of Lee *et al.* [30] and Jang *et al.* [31], result in relatively small deviations for the $\bar{h}$ and Re_{film} ranges. As shown in Fig. 13(a and b), the correlations of Dehbi (1991, 2015) [22], [68] provide MAEs of < 20.8 % for $\bar{h} < 5000$ W/m^2·K and all Re_{film} ranges and slightly increased MAEs of 24.6 % and 27.7 % for $5000 \leq \bar{h} < 10{,}000$ W/m^2·K. Furthermore, the proposed regression model shows MAEs of <18.5 % for all $\bar{h}$ and Re_{film} ranges. The MLP model results in MAEs of < 6.3 % for all $\bar{h}$ and Re_{film} ranges except an MAE of 19.5 % for $5000 \leq \bar{h} < 10{,}000$ W/m^2·K. The poor prediction for $5000 \leq \bar{h} < 10{,}000$ W/m^2·K is due to the lack of data points. In addition, the MLP model provides good predictions for the pure-water vapor data; the MAEs are 2.3 % and 2.4 % for $\bar{h} \geq 10{,}000$ W/m^2·K.

4. Conclusions

This study concerns the condensation heat transfer in the presence of non-condensable gases in a PCCS. Therefore, 826 data points of non-condensable gases and water vapor mixtures and 30 data points of

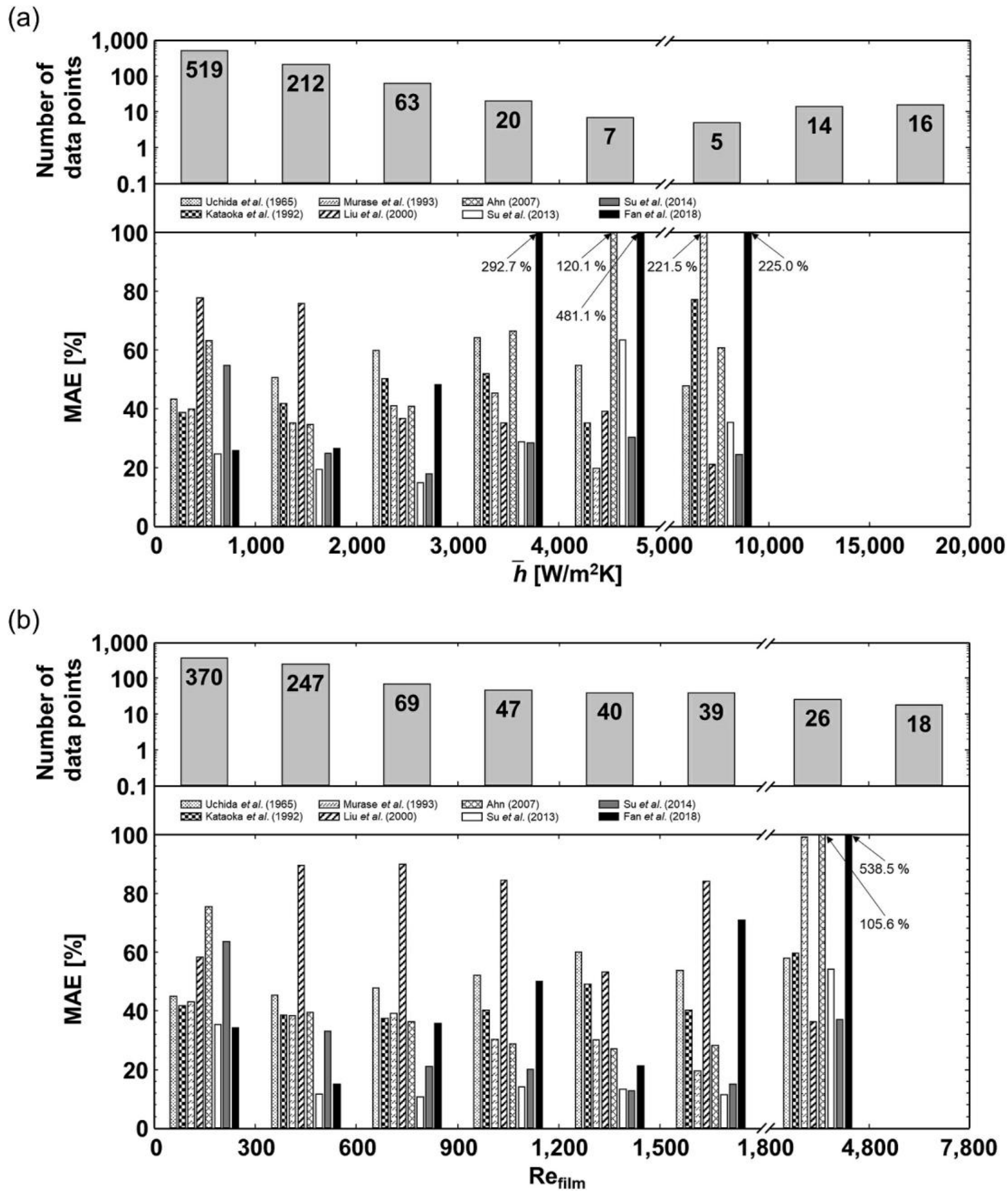

Fig. 12. Distribution of MAEs for predictions with the first group of correlations for the consolidated database relative to (a) average heat transfer coefficient ($\overline{h}$) and (b) the film Reynolds number (Re_{film}).

pure water vapor from 12 literature sources were chosen to investigate the condensation of free-falling films on circular tubes. The investigated non-condensable gases include air and nitrogen; all data covered the following geometrical and operational parameter ranges: $0 \leq W_{nc} \leq 0.9$, $10 \leq D_h \leq 41.2$ mm, $0.3 \leq L \leq 3.5$ m, $0.15 \leq P_{tot} \leq 2.0$ MPa, $5 \leq \Delta T_{sub} \leq 71$ K, $90 \leq \overline{h} \leq 19{,}400$ W/m^2·K, and $8 \leq Re_{film} \leq 7160$. A regression and MLP neural network models for predicting the heat transfer coefficients based on a consolidated database were proposed. In addition, eight relevant correlations without geometrical parameters and four relevant correlations that consider the geometrical parameters were investigated and compared for accuracy with the consolidated database. Among the correlations of the first group, that of Su *et al.* (2013) [27] showed the most accurate predictions with an overall MAE of 23.0 %. Among the correlations of the second group, that of Dehbi (1991) [22] showed the most accurate predictions with an overall MAE of 13.0 %. A new regression model is proposed with a GRG non-linear algorithm by considering the influence of the partial pressure on the average heat transfer coefficient. The proposed regression model showed a slightly improved overall MAE (12.7 %) compared to the best predictions among existing correlations achieved by Dehbi (1991) [22]. In addition, an MLP neural network model was developed to improve the predictability. The architecture included six hidden layers with 26 nodes in each hidden layer. The MLP model resulted in superior predictions with an overall MAE of 4.2 %; all predicted data points had MAEs within ±50 % of the experimentally measured average heat transfer coefficients. The accuracy of the MLP model was compared to the prediction accuracies of the correlations with respect to different ranges of the geometrical and operating conditions. According to the results, the MLP model exhibited evenly outstanding predictions for all geometrical and operation ranges; however, a slightly poor accuracy was observed for $5000 \leq \overline{h} < 10{,}000$ W/m^{2}K because the consolidated database contained only few data points for this range.

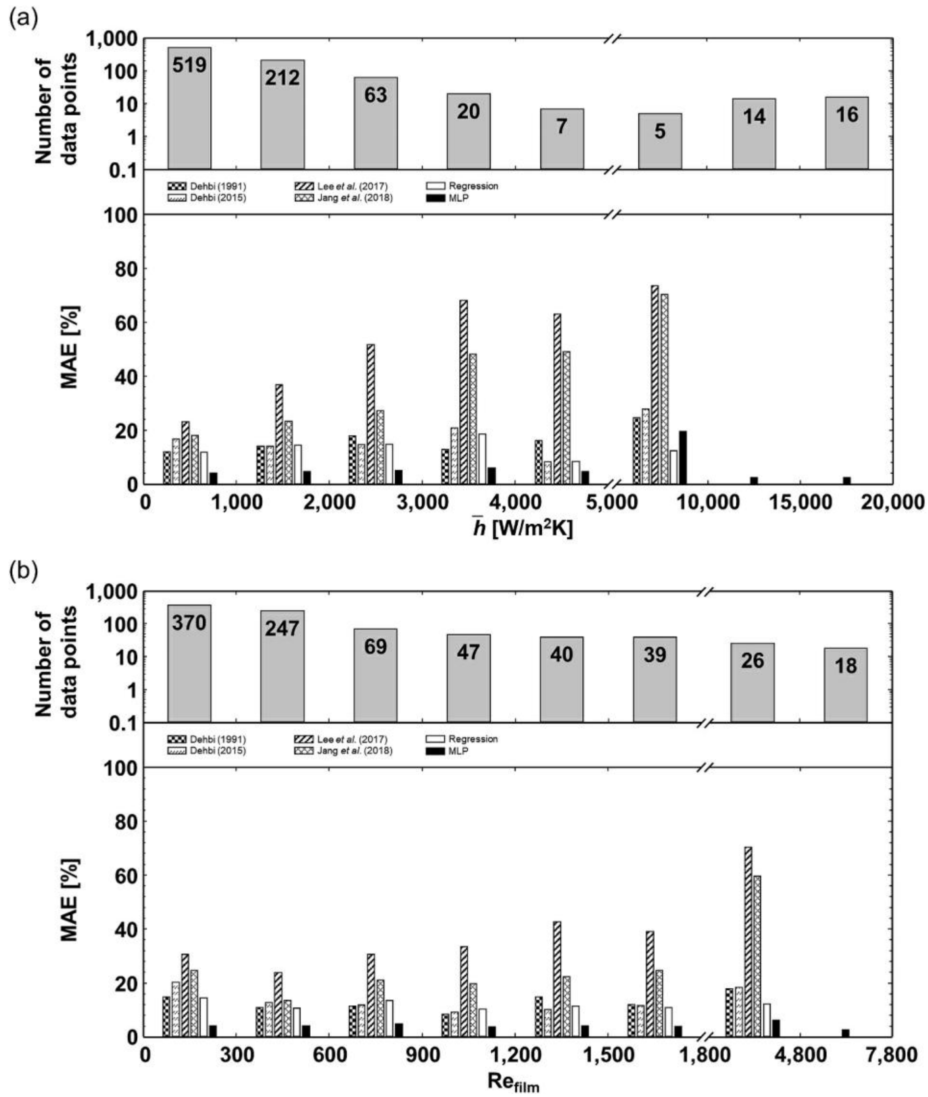

Fig. 13. Distribution of MAEs in predictions of second group of correlations and proposed models for consolidated database relative to (a) the average heat transfer coefficient ($\bar{h}$) and (b) the film Reynolds number (Re_{film}).

Declaration of competing interest

The authors declare that they have no known competing financial interests or personal relationships that could have appeared to influence the work reported in this paper.

Acknowledgment

This research was supported by the Samsung Research Funding & Incubation Center of Samsung Electronics under project number SRFC-TA1903−06 and the Chung-Ang University Graduate Research Scholarship in 2020.

References

[1] International Energy Agency, World Energy Outlook, OECD/IEA, Paris, 2019.
[2] T.J. Yasunari, A. Stohl, R.S. Hayano, J.F. Burkhart, S. Eckhardt, T. Yasunari, Cesium-137 deposition and contamination of Japanese soils due to the Fukushima nuclear accident, Proc. Natl. Acad. Sci. U.S.A. 108 (2011) 19530–19534, https://doi.org/10.1073/pnas.1112058108.
[3] S.N. Tower, T.L. Schulz, R.P. Vijuk, Passive and simplified system features for the advanced Westinghouse 600 MWe PWR, Nucl. Eng. Des. 109 (1988) 147–154, https://doi.org/10.1016/0029-5493(88)90153-7.
[4] T.L. Schulz, Westinghouse AP1000 advanced passive plant, Nucl. Eng. Des. 236 (2006) 1547–1557, https://doi.org/10.1016/j.nucengdes.2006.03.049.
[5] W. Zhou, B. Wolf, S. Revankar, Assessment of RELAP5/MOD3.3 condensation models for the tube bundle condensation in the PCCS of ESBWR, Nucl. Eng. Des. 264 (2013) 111–118, https://doi.org/10.1016/j.nucengdes.2012.08.041.
[6] A.M. Bakhmet'ev, M.A. Bol'shukhin, V.V. Vakhrushev, A.M. Khizbullin, O. V. Makarov, V.V. Bezlepkin, S.E. Semashko, I.M. Ivkov, Experimental validation of the cooling loop for a passive system for removing heat from the AES-2006 protective envelope design for the Leningradskaya nuclear power plant site, Atom. Energy 106 (2009) 185–190, https://doi.org/10.1007/s10512-009-9150-1.
[7] J. Xing, D. Song, Y. Wu, HPR1000: advanced pressurized water reactor with active and passive safety, Engineering 2 (2016) 79–87, https://doi.org/10.1016/J.ENG.2016.01.017.
[8] S.W. Lee, S. Heo, H.U. Ha, H.G. Kim, The concept of the innovative power reactor, Nucl. Eng. Technol. 49 (2017) 1431–1441, https://doi.org/10.1016/j.net.2017.06.015.
[9] H. Ha, S. Lee, H. Kim, Optimal design of passive containment cooling system for innovative PWR, Nucl. Eng. Technol. 49 (2017) 941–952, https://doi.org/10.1016/j.net.2017.03.005.
[10] F.P. Incropera, A.S. Lavine, D.P. DeWitt, Fundamentals of Heat and Mass Transfer, seventh ed., John Wiley & Sons, New York, 2011.
[11] W. Nusselt, Die Oberflächenkondensation des Wasserdampfes, VDI-Z (Ver. Dtsch. Ingenieure-Z) 60 (1916) 541–569.
[12] W.M. Rohsenow, Heat transfer and temperature distribution in laminar film condensation, Trans. Am. Soc. Mech. Eng. 78 (1956) 1645–1648.
[13] R.I. Hirshburg, L.W. Florschuetz, Laminar wavy-film flow: Part II, condensation and evaporation, J. Heat Tran. 104 (1982) 459–464, https://doi.org/10.1115/1.3245115.
[14] W. McAdams, Heat Transmission, third ed., McGraw-Hill, New York, 1954.
[15] S.S. Kutateladze, I.I. Gogonin, Heat transfer in film condensation of slowly moving vapour, Int. J. Heat Mass Tran. 22 (1979) 1593–1599, https://doi.org/10.1016/0017-9310(79)90075-9.

[16] S.S. Kutateladze, Fundamentals of Heat Transfer, Academic Press, New York, 1963.
[17] J.R. Thome, Encyclopedia of Two-phase Heat Transfer and Flow I - Fundamentals and Methods, World Scientific Publishing Co. Pte. Ltd., 2015.
[18] R. Gregorig, J. Kern, K. Turek, Improved correlation of film condensation data based on a more rigorous application of similarity parameters, Wärme- und Stoffübertragung 7 (1974) 1–13, https://doi.org/10.1007/BF01438315.
[19] M.H. Chun, K.T. Kim, Assessment of the new and existing correlations for laminar and turbulent film condensations on a vertical surface, Int. Commun. Heat Mass Tran. 17 (1990) 431–441, https://doi.org/10.1016/0735-1933(90)90062-O.
[20] H. Lee, I. Mudawar, M.M. Hasan, Experimental and theoretical investigation of annular flow condensation in microgravity, Int. J. Heat Mass Tran. 61 (2013) 293–309, https://doi.org/10.1016/j.ijheatmasstransfer.2013.02.010.
[21] J.G. Collier, Convective Boiling and Condensation, second ed., McGraw-Hill, New York, 1981.
[22] A. Dehbi, Analytical and Experimental Investigation of the Effects of Noncondensable Gases on Steam Condensation under Turbulent Natural Convection Conditions, MIT. Department of Nuclear Engineering, Cambridge, MA, 1991. Ph.D. dissertation.
[23] H. Liu, N.E. Todreas, M.J. Driscoll, An experimental investigation of a passive cooling unit for nuclear plant containment, Nucl. Eng. Des. 199 (2000) 243–255, https://doi.org/10.1016/S0029-5493(00)00229-6.
[24] H. Ahn, Experimental Study on the Condensation Heat Transfer with Noncondensable Gas at High Pressure Using Raman Spectroscopy, Master's thesis, Seoul National University, Department of Energy Systems Engineering, Seoul, 2007.
[25] J.W. Kim, Y.G. Lee, H.K. Ahn, G.C. Park, Condensation heat transfer characteristic in the presence of noncondensable gas on natural convection at high pressure, Nucl. Eng. Des. 239 (2009) 688–698, https://doi.org/10.1016/j.nucengdes.2008.12.011.
[26] M. Kawakubo, M. Aritomi, H. Kikura, T. Komeno, An experimental study on the cooling characteristics of passive containment cooling systems, J. Nucl. Sci. Technol. 46 (2009) 7, https://doi.org/10.1080/18811248.2007.9711539.
[27] J. Su, Z. Sun, G. Fan, M. Ding, Experimental study of the effect of non-condensable gases on steam condensation over a vertical tube external surface, Nucl. Eng. Des. 262 (2013) 201–208, https://doi.org/10.1016/j.nucengdes.2013.05.002.
[28] J. Su, Z. Sun, M. Ding, G. Fan, Analysis of experiments for the effect of noncondensable gases on steam condensation over a vertical tube external surface under low wall subcooling, Nucl. Eng. Des. 278 (2014) 644–650, https://doi.org/10.1016/j.nucengdes.2014.07.022.
[29] P. Tong, G. Fan, Z. Sun, M. Ding, J. Su, An experimental investigation of pure steam and steam–air mixtures condensation outside a vertical pin-fin tube, Exp. Therm. Fluid Sci. 69 (2015) 141–148, https://doi.org/10.1016/j.expthermflusci.2015.08.009.
[30] Y.G. Lee, Y.J. Jang, D.J. Choi, An experimental study of air–steam condensation on the exterior surface of a vertical tube under natural convection conditions, Int. J. Heat Mass Tran. 104 (2017) 1034–1047, https://doi.org/10.1016/j.ijheatmasstransfer.2016.09.016.
[31] Y.J. Jang, D.J. Choi, S. Kim, D.W. Jerng, Y.G. Lee, Development of an empirical correlation for condensation heat transfer coefficient on a vertical tube in the presence of a noncondensable gas, KSME-B. 42 (2018) 187–196, https://doi.org/10.3795/KSME-B.2018.42.3.187.
[32] G. Fan, P. Tong, Z. Sun, Y. Chen, Experimental study of pure steam and steam–air condensation over a vertical corrugated tube, Prog. Nucl. Energy 109 (2018) 239–249, https://doi.org/10.1016/j.pnucene.2018.08.020.
[33] G. Fan, P. Tong, Z. Sun, Y. Chen, Development of a new empirical correlation for steam condensation rates in the presence of air outside vertical smooth tube, Ann. Nucl. Energy 113 (2018) 139–146, https://doi.org/10.1016/j.anucene.2017.11.021.
[34] M. Olson, A. Wyner, R. Berk, Modern neural networks generalize on small data sets, Adv. Neural Inf. Process. Syst. 31 (2018) 3619–3628.
[35] D.H. Fisher, Knowledge acquisition via incremental conceptual clustering, Mach. Learn. 2 (1987) 139–172, https://doi.org/10.1007/BF00114265.
[36] J.R. Koza, Genetic Programming: on the Programming of Computers by Means of Natural Selection, The MIT Press, London, UK, 1992.
[37] S.K. Murthy, Automatic construction of decision trees from data: a multi-disciplinary survey, Data Min. Knowl. Discov. 2 (1998) 345–389.
[38] Y. LeCun, Y. Bengio, G. Hinton, Deep learning, Nature 521 (2015) 436–444, https://doi.org/10.1038/nature14539.
[39] W.S. McCulloch, W. Pitts, A logical calculus of the ideas immanent in nervous activity, Bull. Math. Biophys. 5 (1943) 115–133, https://doi.org/10.1007/BF02478259.
[40] P.J. Werbos, Beyond Regression: New Tools for Prediction and Analysis in the Behavioral Sciences, Harvard University, Boston, MA, 1974. Ph.D. thesis.
[41] D.E. Rumelhart, G.E. Hinton, R.J. Williams, Learning representations by back-propagating errors, Nature 323 (1986) 533–536, https://doi.org/10.1038/323533a0.
[42] H. Lee, C.R. Kharangate, N. Mascarenhas, I. Park, I. Mudawar, Experimental and computational investigation of vertical downflow condensation, Int. J. Heat Mass Tran. 85 (2015) 865–879, https://doi.org/10.1016/j.ijheatmasstransfer.2015.02.037.
[43] K. Jambunathan, S.L. Hartle, S. Ashforth-Frost, V.N. Fontama, Evaluating convective heat transfer coefficients using neural networks, Int. J. Heat Mass Tran. 39 (1996) 2329–2332, https://doi.org/10.1016/0017-9310(95)00332-0.
[44] A. Pacheco-Vega, M. Sen, K.T. Yang, R.L. McClain, Neural network analysis of fin-tube refrigerating heat exchanger with limited experimental data, Int. J. Heat Mass Tran. 44 (2001) 763–770, https://doi.org/10.1016/S0017-9310(00)00139-3.
[45] Y. Islamoglu, A. Kurt, Heat transfer analysis using ANNs with experimental data for air flowing in corrugated channels, Int. J. Heat Mass Tran. 47 (2004) 1361–1365, https://doi.org/10.1016/j.ijheatmasstransfer.2003.07.031.
[46] A.M. Ghahdarijani, F. Hormozi, A.H. Asl, Convective heat transfer and pressure drop study on nanofluids in double-walled reactor by developing an optimal multilayer perceptron artificial neural network, Int. Commun. Heat Mass Tran. 84 (2017) 11–19, https://doi.org/10.1016/j.icheatmasstransfer.2017.03.014.
[47] P. Naphon, S. Wiriyasart, T. Arisariyawong, L. Nakharintr, ANN, numerical and experimental analysis on the jet impingement nanofluids flow and heat transfer characteristics in the micro-channel heat sink, Int. J. Heat Mass Tran. 131 (2019) 329–340, https://doi.org/10.1016/j.ijheatmasstransfer.2018.11.073.
[48] H. Lee, M. Kang, K.W. Jung, C.R. Kharangate, S. Lee, M. Iyengar, C. Malone, M. Asheghi, K.E. Goodson, H. Lee, An artificial neural network model for predicting frictional pressure drop in micro-pin fin heat sink, Appl. Therm. Eng. 194 (2021) 117012, https://doi.org/10.1016/j.applthermaleng.2021.117012.
[49] M. Stone, Cross-validatory choice and assessment of statistical predictions, J. Roy. Stat. Soc. B36 (1974) 111–133, https://doi.org/10.1111/j.2517-6161.1974.tb00994.x.
[50] M. Balcilar, A.S. Dalkilic, S. Wongwises, Artificial neural network techniques for the determination of condensation heat transfer characteristics during downward annular flow of R134a inside a vertical smooth tube, Int. Commun. Heat Mass Tran. 38 (2011) 75–84, https://doi.org/10.1016/j.icheatmasstransfer.2010.10.009.
[51] S. Azizi, E. Ahmadloo, Prediction of heat transfer coefficient during condensation of R134a in inclined tubes using artificial neural network, Appl. Therm. Eng. 106 (2016) 203–210, https://doi.org/10.1016/j.applthermaleng.2016.05.189.
[52] A. Khosravi, J.J.G. Pabon, R.N.N. Koury, L. Machado, Using machine learning algorithms to predict the pressure drop during evaporation of R407C, Appl. Therm. Eng. 133 (2018) 361–370, https://doi.org/10.1016/j.applthermaleng.2018.01.084.
[53] A. Parrales, J. Hernández-Pérez, O. Flores, H. Hernandez, J. Gómez-Aguilar, R. Escobar-Jiménez, A. Huicochea, Heat transfer coefficients analysis in a helical double-pipe evaporator: Nusselt number correlations through artificial neural networks, Entropy 21 (2019) 689, https://doi.org/10.3390/e21070689.
[54] Y. Qiu, D. Garg, L. Zhou, C.R. Kharangate, S.-M. Kim, I. Mudawar, An artificial neural network model to predict mini/micro-channels saturated flow boiling heat transfer coefficient based on universal consolidated data, Int. J. Heat Mass Tran. 149 (2020) 119211, https://doi.org/10.1016/j.ijheatmasstransfer.2019.119211.
[55] L. Zhou, D. Garg, Y. Qiu, S.-M. Kim, I. Mudawar, C.R. Kharangate, Machine learning algorithms to predict flow condensation heat transfer coefficient in mini/micro-channel utilizing universal data, Int. J. Heat Mass Tran. 162 (2020) 120351, https://doi.org/10.1016/j.ijheatmasstransfer.2020.120351.
[56] G. Zhu, T. Wen, D. Zhang, Machine learning based approach for the prediction of flow boiling/condensation heat transfer performance in mini channels with serrated fins, Int. J. Heat Mass Tran. 166 (2021) 120783, https://doi.org/10.1016/j.ijheatmasstransfer.2020.120783.
[57] H. Uchida, A. Oyama, Y. Togo, Evaluation of post-incident cooling systems of light-water power reactors, Proc. 3rd Int. Conf. on the Peaceful Uses of Atomic Energy 13 (1965) 93–102.
[58] Y. Kataoka, T. Fukui, S. Hatamiya, T. Nakao, M. Naitoh, I. Sumida, Experiments on convection heat transfer along a vertical flat plate between pools with different temperatures, Nucl. Technol. 99 (1992) 386–396, https://doi.org/10.13182/NT92-A34722.
[59] M. Murase, Y. Kataoka, T. Fujii, Evaporation and condensation heat transfer with a noncondensable gas present, Nucl. Eng. Des. 141 (1993) 135–143, https://doi.org/10.1016/0029-5493(93)90098-T.
[60] S. Chapman, T.G. Cowling, The Mathematical Theory of Non-uniform Gases, third ed., Cambridge University Press, Cambridge, 1970.
[61] R. Cebeci, Laminar-free-convective-heat transfer from the outer surface of a vertical slender circular cylinder, Proc. 5th Int. Heat Transfer Conf. 3 (1974) 15–19. Paper NC 1.4.
[62] L.S. Lasdon, A.D. Waren, A. Jain, M. Ratner, Design and testing of a generalized reduced gradient code for nonlinear programming, ACM Trans. Math Software 4 (1978) 34–50, https://doi.org/10.1145/355769.355773.
[63] K. Pearson, Notes on regression and inheritance in the case of two parents, Proc. Roy. Soc. Lond. 58 (1895) 240–242, https://doi.org/10.1098/rspl.1895.0041.
[64] A.L. Maas, A.Y. Hannun, A.Y. Ng, Rectifier nonlinearities improve neural network acoustic models, in: 30th Int. Conf. on Machine Learning, 2013, pp. 3–11, 30.
[65] K. He, X. Zhang, S. Ren, J. Sun, Delving deep into rectifiers: surpassing human-level performance on ImageNet classification, in: 2015 IEEE International Conference on Computer Vision (ICCV), IEEE, Santiago, Chile, 2015, pp. 1026–1034, https://doi.org/10.1109/ICCV.2015.123.
[66] D.P. Kingma, J. Ba, Adam, A method for stochastic optimization, in: Proc. 3rd Int. Conf. On Learning Representations, 2015. San Diego, CA, USA.
[67] P.F. Peterson, Theoretical basis for the Uchida correlation for condensation in reactor containments, Nucl. Eng. Des. 162 (1996) 301–306, https://doi.org/10.1016/0029-5493(95)01125-0.
[68] A. Dehbi, A generalized correlation for steam condensation rates in the presence of air under turbulent free convection, Int. J. Heat Mass Tran. 86 (2015) 1–15, https://doi.org/10.1016/j.ijheatmasstransfer.2015.02.034.